

Simultaneously Updating All Persistence Values in Reinforcement Learning

Luca Sabbioni¹, Luca Al Daire¹, Lorenzo Bisi², Alberto Maria Metelli¹, Marcello Restelli¹

¹Politecnico di Milano, Milan, Italy

²ML cube, Milan, Italy

luca.sabbioni@polimi.it

Abstract

In *reinforcement learning*, the performance of learning agents is highly sensitive to the choice of time discretization. Agents acting at high frequencies have the best control opportunities, along with some drawbacks, such as possible inefficient exploration and vanishing of the action advantages. The repetition of the actions, i.e., *action persistence*, comes into help, as it allows the agent to visit wider regions of the state space and improve the estimation of the action effects. In this work, we derive a novel *All-Persistence Bellman Operator*, which allows an effective use of both the low-persistence experience, by decomposition into sub-transition, and the high-persistence experience, thanks to the introduction of a suitable *bootstrap* procedure. In this way, we employ transitions collected at *any* time scale to update simultaneously the action values of the considered persistence set. We prove the contraction property of the All-Persistence Bellman Operator and, based on it, we extend classic Q-learning and DQN. After providing a study on the effects of persistence, we experimentally evaluate our approach in both tabular contexts and more challenging frameworks, including some Atari games.

1 Introduction

In recent years, Reinforcement Learning (RL, Sutton and Barto 2018) methods have proven to be successful in a wide variety of applications, including robotics (Kober and Peters 2014; Gu et al. 2017; Haarnoja et al. 2019; Kilinc, Hu, and Montana 2019), autonomous driving (Kiran et al. 2021) and continuous control (Lillicrap et al. 2016; Schulman et al. 2017). These sequential decision-making problems are typically modelled as a Markov Decision Process (MDP, Puterman 2014), a formalism that addresses the agent-environment interactions through *discrete-time* transitions. *Continuous-time* control problems, instead, are usually addressed by means of time discretization, which induces a specific control frequency f , or, equivalently, a time step $\delta = \frac{1}{f}$ (Park, Kim, and Kim 2021). This represents an environment hyperparameter, which may have dramatic effects on the process of learning the optimal policy (Metelli et al. 2020; Kalyanakrishnan et al. 2021). Indeed, higher frequencies allow for greater control opportunities, but they have significant drawbacks.

The most relevant one is related to the toned down effect of the selected actions. In the limit for time discretization $\delta \rightarrow 0$, the advantage of each action collapses to zero, preventing the agent from finding the best action (Baird 1994; Tallec, Blier, and Ollivier 2019). Even policy gradient methods are shown to fail in this (near-)continuous-time setting, and the reason is related to the divergent variance of the gradient (Park, Kim, and Kim 2021). The consequences of each action might be detected if the dynamics of the environment has the time to evolve, hence with an agent acting with higher frequencies lead to higher sample complexity.

Another consequence of the use of high frequencies is related to the difficulty of exploration. A random uniform policy played at high frequency may not be adequate, as in some classes of environments, including the majority of real-world control problems, it tends to visit only a local neighborhood of the initial state (Amin et al. 2021; Park, Kim, and Kim 2021; Yu, Xu, and Zhang 2021). This is problematic, especially in goal-based or sparse rewards environments, where the most informative states may never be visited. On the other hand, large time discretizations benefit from a higher probability of reaching far states, but they also deeply modify the transition process, hence a possibly large subspace of states may not be reachable.

One of the solutions to achieve the advantages related to exploration and sample complexity, while keeping the control opportunity loss bounded, consists in *action persistence* or *action repetition* (Schoknecht and Riedmiller 2003; Braylan et al. 2015; Lakshminarayanan, Sharma, and Ravindran 2017; Metelli et al. 2020), which is equivalent to acting at lower frequencies. Thus, the agent can achieve, in some environments, a more effective exploration, better capture the consequences of each action, and fasten convergence to the optimal policy.

In this work, we propose a value-based approach in which the agent does not only choose the *action*, but also its *persistence*, with the goal of making the most effective use of samples collected at different persistences. The main contribution of this paper is a general approach in which information collected from the interaction with the environment at *one* persistence is used to improve the action value function estimates of *all* the considered possible persistences. On one hand, the $\bar{\kappa}$ -step transitions can be decomposed in many sub-transitions of reduced length and used to update

lower persistence $k \leq \bar{k}$ value functions. On the other hand, they represent partial information for the estimation of the effects of higher persistence $k > \bar{k}$ actions. Indeed, they can be employed to update the estimates by using a suitable *bootstrapping* procedure of the missing information. This means that, after the interaction with the environment, according to the action-persistence pair selected by the agent, all value function estimates are updated simultaneously for each of the available persistences $k \in \mathcal{K}$. We formalize, in Section 4, this procedure by introducing the *All-persistence Bellman Operator*. We prove that such an operator enjoys a contraction property analogous to that of the traditional optimal Bellman operator. Consequently, in Section 5 we embed the All-persistence Bellman operator into the classic Q-learning algorithm, obtaining *Persistent Q-learning* (PerQ-learning). This novel algorithm, through an effective use of the transitions sampled at different persistences, displays two main advantages. First, since each individual transition is employed to update the value function estimates at different persistences, we experience a faster convergence. Second, the execution of persistent actions, given the nature of a large class of environments, fosters exploration of the state space, with a direct effect on the learning speed (Section 6). Furthermore, to deal with more complex domains, we move, in Section 7, to the Deep RL scenario, extending the Deep Q-Network (DQN) algorithm to its persistent version, called *Persistent Deep Q-Network* (PerDQN). Finally, in Section 8, we evaluate the proposed algorithms, in comparison with state-of-the-art approaches, on illustrative and complex domains, highlighting strengths and weaknesses.

2 Related Work

The first work extending RL agents with action repetition, go back to Schoknecht and Riedmiller 2003. In this paper, multi-step actions (MSAs) were introduced, reducing the number of decisions needed to reach the goal and making the time scale coarser. Action persistence has acquired practical relevance since the introduction of Deep RL (Mnih et al. 2013), by leveraging the *frame skip* parameter (Bellemare et al. 2013). Several works (Braylan et al. 2015; Khan et al. 2019; Metelli et al. 2020) had shown the importance of persistence for helping exploration and policy learning. Among these works, Dabney, Ostrovski, and Barreto 2020 introduced an ϵz -greedy exploration, with a random exploratory variable deciding the duration of each action. As explained in Metelli et al. 2020, changing frequency deeply modifies the underlying MDP, as a special instance of a configurable MDP (Metelli, Mutti, and Restelli 2018), where environmental parameters can be tuned to improve the performance. Indeed, in Grigsby, Yoo, and Qi 2021 the authors proposed an algorithm to automatically tune the control frequency, along with other learning hyperparameters. Mann, Mannor, and Precup 2015 illustrates that approximate value iteration techniques can converge faster with action persistence (seen as *options* with longer duration).

Action repetition has many advantages, but it may reduce the control opportunities. Consequently, researchers have been trying to include the possibility to *dynamically* change

the control frequency during learning: in Augmented-DQN (Lakshminarayanan, Sharma, and Ravindran 2017), the action space is duplicated to be able to choose actions with two previously selected repetition rates.

A different approach is proposed in Sharma, Srinivas, and Ravindran 2017, where a *skip network* is used to the action persistence in a specific state, regardless of the chosen action. One way to differentiate persistences with actions is proposed by TempoRL (Biedenkapp et al. 2021), where the skip network depends on both state and action (and the estimated Q-value function) to evaluate the effects for different possible frequencies. In G. Bellemare et al. 2016, *persistent advantage learning* is proposed in which the advantage learning is overridden by a Q-learning update with repeated actions, when the latter promises better Q-values.

In the framework of policy-gradient methods, persistence is introduced in Yu, Xu, and Zhang 2021, with the introduction of a secondary policy for choosing whether to repeat the previous action or to change it according to the principal agent. A completely different approach is presented by Park, Kim, and Kim 2021: the authors claim that when $\delta \rightarrow 0$ policy-based methods tend to degrade. Thanks to the introduction of a *safe region*, the agent keeps repeating an action until the distance of the visited states overcomes a certain threshold. This state locality can guarantee reactivity, especially in some environments where the blind repetition of an action can be dangerous.

3 Preliminaries

In this section, we provide the necessary background employed in the following of the paper.

Mathematical Background Given a measurable space $(\mathcal{X}, \sigma_{\mathcal{X}})$, where \mathcal{X} is a set and $\sigma_{\mathcal{X}}$ a σ -algebra, we denote with $\mathcal{P}(\mathcal{X})$ the set of probability measures and with $\mathcal{B}(\mathcal{X})$ the set of the bounded measurable functions. We denote with δ_x the Dirac measure centered in $x \in \mathcal{X}$. Let $f \in \mathcal{B}(\mathcal{X})$, the L_{∞} -norm is defined as $\|f\|_{\infty} = \sup_{x \in \mathcal{X}} f(x)$.

Markov Decision Processes A discrete-time Markov Decision Process (MDP, Puterman 2014) is defined as a tuple $\mathcal{M} := \langle \mathcal{S}, \mathcal{A}, P, r, \gamma \rangle$, where \mathcal{S} is the state space, \mathcal{A} the finite action space, $P : \mathcal{S} \times \mathcal{A} \rightarrow \mathcal{P}(\mathcal{S})$ is the Markovian transition kernel, $r : \mathcal{S} \times \mathcal{A} \rightarrow \mathbb{R}$ is the reward function, bounded as $\|r\|_{\infty} \leq R_{\max} < +\infty$, and $\gamma \in [0, 1)$ is the discount factor. A Markovian stationary policy $\pi : \mathcal{S} \rightarrow \mathcal{P}(\mathcal{A})$ maps states to probability measures over \mathcal{A} . We denote with Π the set of Markovian stationary policies. The *action-value function*, or *Q-function*, of a policy $\pi \in \Pi$ is the expected discounted sum of the rewards obtained by performing action a in state s and following policy π thereafter: $Q^{\pi}(s, a) = \mathbb{E}_{\pi} [\sum_{t=0}^{+\infty} \gamma^t r_{t+1} | s_0 = s, a_0 = a]$, where $r_{t+1} = r(s_t, a_t)$, $a_t \sim \pi(\cdot | s_t)$, and $s_{t+1} \sim P(\cdot | s_t, a_t)$ for all $t \in \mathbb{N}$. The optimal Q-function is given by: $Q^*(s, a) = \sup_{\pi \in \Pi} Q^{\pi}(s, a)$ for all $(s, a) \in \mathcal{S} \times \mathcal{A}$. A policy π is *greedy* w.r.t. a function $f \in \mathcal{B}(\mathcal{S} \times \mathcal{A})$ if it plays only greedy actions, i.e., $\pi(\cdot | s) \in \mathcal{P}(\arg \max_{a \in \mathcal{A}} f(s, a))$. An *optimal policy* $\pi^* \in \Pi$ is any policy greedy w.r.t. Q^* .

Algorithm 1: All Persistence Bellman Update

Require: Sampling persistence \bar{k}_t , partial history $H_t^{\bar{k}_t}$,
Q-function Q .

Ensure: Updated Q-function Q

```
1: for  $j=\bar{k}_t, \bar{k}_t-1, \dots, 1$  do
2:   for  $i=j-1, j-2, \dots, 0$  do
3:      $k \leftarrow j-i$ 
4:      $Q(s_{t+i}, a_t, k) \leftarrow (1-\alpha)Q(s_{t+i}, a_t, k) +$ 
5:        $\alpha \widehat{T}_{t+i}^k Q(s_{t+i}, a_t, k)$ 
6:     for  $d=1, 2, \dots, K_{\max}-k$  do
7:        $Q(s_{t+i}, a_t, k+d) \leftarrow (1-\alpha)Q(s_{t+i}, a_t, k+d) +$ 
8:          $\alpha \widehat{T}_{t+i}^k Q(s_{t+i}, a_t, k+d)$ 
9:     end for
10:  end for
11: end for
```

Q-learning The *Bellman Optimal Operator* $T^* : \mathcal{B}(\mathcal{S} \times \mathcal{A}) \rightarrow \mathcal{B}(\mathcal{S} \times \mathcal{A})$ is defined for every $f \in \mathcal{B}(\mathcal{S} \times \mathcal{A})$ and $(s, a) \in \mathcal{S} \times \mathcal{A}$ as in (Bertsekas and Shreve 1996): $(T^*f)(s, a) = r(s, a) + \gamma \int_{\mathcal{S}} P(ds'|s, a) \max_{a' \in \mathcal{A}} f(s', a')$. T^* is a γ -contraction in L_∞ -norm and its unique fixed point is the optimal Q-function. When P and r are known, value-iteration (Puterman 2014) allows computing Q^* via iterative application of T^* . When the environment is unknown, Q-learning (Watkins 1989) collects samples with a *behavioral* policy (e.g., ϵ -greedy) and then updates Q-function estimate based on the updated rule: $Q(s_t, a_t) \leftarrow (1-\alpha)Q(s_t, a_t) + \alpha(r_{t+1} + \gamma \max_{a' \in \mathcal{A}} Q(s_{t+1}, a'))$. where $\alpha > 0$ is the learning rate.

Deep Q-Networks Deep Q-Network (DQN, Mnih et al. 2013, 2015) employs a deep neural network with weights θ to learn an approximation Q_θ of Q^* . The transitions are stored in the *replay buffer* $\mathcal{D} = \{(s_t, a_t, r_{t+1}, s_{t+1})\}_{t=1}^n$ to mitigate temporal correlations. To improve stability, a *target network*, whose parameters θ^- are kept fixed for a certain number of steps, is employed. The Q-Network is trained to minimize the mean squared temporal difference error $r + \gamma \max_{a' \in \mathcal{A}} Q_{\theta^-}(s', a') - Q_\theta(s, a)$ on a batch of tuples sampled from the replay buffer $(s, a, r, s') \sim \mathcal{D}$.

Action Persistence The execution of actions with a persistence $k \in \mathbb{N}$ can be modeled by means of the k -persistent MDP (Metelli et al. 2020), characterized by the k -persistent transition model P_k and reward function r_k . To formally define them, the *persistent transition model* is introduced: $P^\delta(\cdot, \cdot | s, a) = \int_{\mathcal{S}} P(ds' | s, a) \delta_{(s', a)}(\cdot, \cdot)$, which replicates in the next state s' the previous action a . Thus, we have $P_k(\cdot | s, a) = ((P^\delta)^{k-1} P)(\cdot | s, a)$ and $r_k(s, a) = \sum_{i=0}^{k-1} \gamma^i ((P^\delta)^i r)(s, a)$. This framework eases the analysis of *fixed* persistences, but it does not allow action repetition for a *variable* number of steps.

4 All-Persistence Bellman Update

In this section, we introduce our approach to make effective use of the samples collected at *any* persistence. We first introduce the notion of *persistence option* and then, we present the *all-persistence Bellman operator*.

Algorithm 2: Persistent Q-learning (PerQ-learning)

Require: Learning rate α , exploration coefficient ϵ ,
number of episodes N

Ensure: Q-function

```
1: Initialize  $Q$  arbitrarily,  $Q(\text{terminal}, \cdot, \cdot) = 0$ 
2: for  $\text{episode} = 1, \dots, N$  do
3:    $t \leftarrow 0$ 
4:   while  $s_t$  is not terminal do
5:      $a_t, \bar{k}_t \sim \psi_Q^\epsilon(s_t)$ 
6:     for  $\tau = 1, \dots, \bar{k}_t$  do
7:       Take action  $a_t$ , observe  $s_{t+\tau}, r_{t+\tau}$ 
8:     end for
9:     Store partial history  $H_t^{\bar{k}_t}$ 
10:    Update  $Q$  according to Alg.1
11:     $t \leftarrow t + \bar{k}_t$ 
12:  end while
13: end for
```

4.1 Persistence Options

We formalize the decision process in which the agent chooses a primitive action a together with its persistence k . To this purpose, we introduce the *persistence option*.

Definition 4.1 Let \mathcal{A} be the space of primitive actions of an MDP \mathcal{M} and $\mathcal{K} := \{1, \dots, K_{\max}\}$, where $K_{\max} \geq 1$, be the set of persistences. A persistence option $o := (a, k)$ is the decision of playing primitive action $a \in \mathcal{A}$ with persistence $k \in \mathcal{K}$. We denote with $\mathcal{O}^{(k)} := \{(a, k) : a \in \mathcal{A}\}$ the set of options with fixed persistence $k \in \mathcal{K}$ and $\mathcal{O} := \bigcup_{k \in \mathcal{K}} \mathcal{O}^{(k)} = \mathcal{A} \times \mathcal{K}$.

The decision process works as follows. At time $t = 0$, the agent observes $s_0 \in \mathcal{S}$, selects a persistence option $o_0 = (a_0, k_0) \in \mathcal{O}$, observes the sequence of states (s_1, \dots, s_{k_0}) generated by repeating primitive action a_0 for k_0 times, i.e., $s_{i+1} \sim P(\cdot | s_i, a_0)$ for $i \in \{0, \dots, k_0 - 1\}$, and the sequence of rewards (r_1, \dots, r_{k_0}) with $r_{i+1} = r(s_i, a_0)$ for $i \in \{0, \dots, k_0 - 1\}$. Then, in state s_{k_0} the agent selects another option $o_1 = (a_1, k_1) \in \mathcal{O}$ and the process repeats. During the execution of the persistence option, the agent is not allowed to change the primitive action.¹

Remark 4.1 (Persistence and Options) The persistence option (Definition 4.1) is in all regards a semi-Markov option (Precup 2001), where the initiation set is the set of all states \mathcal{S} , the termination condition depends on time only, and the intra-option policy is constant. Indeed, the described process generates a semi-Markov decision process (Puterman 2014), fully determined by the behavior of \mathcal{M} , as shown in (Sutton, Precup, and Singh 1999).

Remark 4.2 (Persistence Options vs Augmented Action Space) There is an important difference between using persistence options \mathcal{O} in the original MDP \mathcal{M} and defining an augmented MDP $\mathcal{M}_{\mathcal{K}}$ with new action space $\mathcal{A} \times \mathcal{K}$ and properly redefined transition model and reward function (Lakshminarayanan, Sharma, and Ravindran 2017): when executing a persistence option $o_t = (a_t, k_t) \in \mathcal{O}$ at time t ,

¹From this definition, it follows that \mathcal{A} is isomorphic to $\mathcal{O}^{(1)}$.

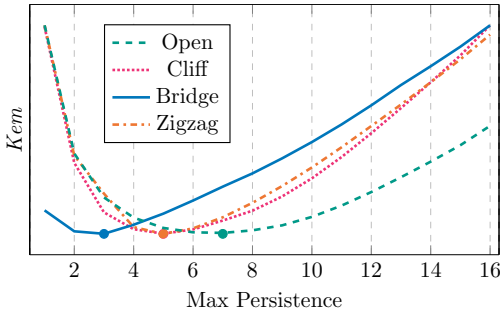


Figure 1: Normalized Kemeny’s constant in tabular environments as function of K_{\max} . Bullets represent the minimum.

we observe the full sequence of states $(s_{t+1}, \dots, s_{t+k_t})$ and rewards $(r_{t+1}, \dots, r_{t+k_t})$. Instead, in the augmented MDP $\mathcal{M}_{\mathcal{K}}$ we only observe the last state s_{k_t} and the cumulative reward $r_{t+1}^k = \sum_{i=0}^{k-1} \gamma^i r_{t+i+1}$. We will heavily exploit the particular option structure, re-using fragments of experience to perform intra-option learning.

We now extend the policy and state-action value function definitions to consider this particular form of options. A Markovian stationary policy over persistence options $\psi : \mathcal{S} \rightarrow \mathcal{P}(\mathcal{O})$ is a mapping between states and probability measures over persistence options. We denote with Ψ the set of the policies of this nature. The state-option value function $Q^\psi : \mathcal{S} \times \mathcal{O} \rightarrow \mathbb{R}$ following a policy over options $\psi \in \Psi$ is defined as $Q^\psi(s, a, k) := \mathbb{E}_\psi \left[\sum_{t=0}^{+\infty} \gamma^t r_{t+1} \mid s_0 = s, a_0 = a, k_0 = k \right]$. In this context, the optimal action-value function is defined as: $Q_{\mathcal{K}}^*(s, a, k) = \sup_{\psi \in \Psi} Q^\psi(s, a, k)$.

4.2 All-Persistence Bellman Operator

Our goal is to leverage any \bar{k} -persistence transition to learn $Q_{\mathcal{K}}^*(\cdot, \cdot, k)$ for all the possible action-persistences in $k \in \mathcal{K}$. Suppose that $\bar{k} \geq k$, then, we can exploit any sub-transition of k steps from the \bar{k} -persistence transition to update the value $Q_{\mathcal{K}}^*(\cdot, \cdot, k)$. Thus, we extend the Bellman optimal operator to persistence options $T^* : \mathcal{B}(\mathcal{S} \times \mathcal{O}) \rightarrow \mathcal{B}(\mathcal{S} \times \mathcal{O})$ with $f \in \mathcal{B}(\mathcal{S} \times \mathcal{O})$:

$$(T^* f)(s, a, k) = r_k(s, a) + \gamma^k \int_{\mathcal{S}} P_k(ds' | s, a) \max_{(a', k') \in \mathcal{O}} f(s', a', k').$$

If, instead, $\bar{k} < k$, in order to update the value $Q_{\mathcal{K}}^*(\cdot, \cdot, k)$, we partially exploit the \bar{k} -persistent transition, but then, we need to bootstrap from a lower persistence Q -value, to compensate the remaining $k - \bar{k}$ steps. To this end, we introduce the bootstrapping operator

$$T^{\bar{k}} : \mathcal{B}(\mathcal{S} \times \mathcal{O}) \rightarrow \mathcal{B}(\mathcal{S} \times \mathcal{O}) \text{ with } f \in \mathcal{B}(\mathcal{S} \times \mathcal{O}):$$

$$(T^{\bar{k}} f)(s, a, k) = r_{\bar{k}}(s, a) + \gamma^{\bar{k}} \int_{\mathcal{S}} P_{\bar{k}}(ds' | s, a) f(s', a, k - \bar{k}).$$

By combining these two operators, we obtain the All-Persistence Bellman operator $\mathcal{H}_{\bar{k}} : \mathcal{B}(\mathcal{S} \times \mathcal{O}) \rightarrow \mathcal{B}(\mathcal{S} \times \mathcal{O})$ defined for every $f \in \mathcal{B}(\mathcal{S} \times \mathcal{O})$ as: $(\mathcal{H}_{\bar{k}} f)(s, a, k) =$

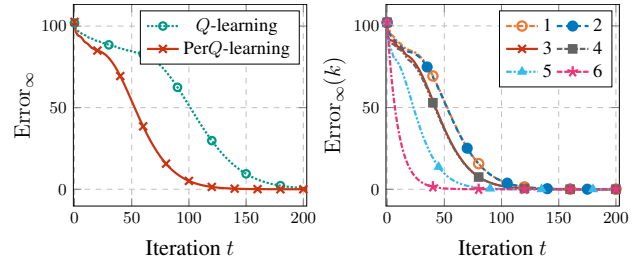


Figure 2: L_∞ error on 6x6 grid-world between synchronous Q -learning and Per Q -learning (left) and for different persistence options $k \in \{1, \dots, 6\}$ of Per Q -learning (right). (100 runs, avg \pm 95 % c.i.)

$((\mathbb{1}_{k \leq \bar{k}} T^* + \mathbb{1}_{k > \bar{k}} T^{\bar{k}}) f)(s, a, k)$. Thus, given a persistence $\bar{k} \in \mathcal{K}$, $\mathcal{H}_{\bar{k}}$ allows updating all the Q -values with $k \leq \bar{k}$ by means of T^* , and all the ones with $k > \bar{k}$ by means of $T^{\bar{k}}$. The following result demonstrates its soundness.

Theorem 4.1 *The all-persistence Bellman operator $\mathcal{H}_{\bar{k}}$ fulfills the following properties:*

1. $\mathcal{H}_{\bar{k}}$ is a γ -contraction in L_∞ norm;
2. $Q_{\mathcal{K}}^*$ is its unique fixed point;
3. $Q_{\mathcal{K}}^*$ is monotonic in k , i.e., for all $(s, a) \in \mathcal{S} \times \mathcal{A}$ if $k \leq k'$ then $Q_{\mathcal{K}}^*(s, a, k) \geq Q_{\mathcal{K}}^*(s, a, k')$.

Thus, operator $\mathcal{H}_{\bar{k}}$ contracts to the optimal action-value function $Q_{\mathcal{K}}^*$, which, thanks to monotonicity, has its highest value at the lowest possible persistence. In particular, it is simple to show that $Q_{\mathcal{K}}^*(s, a, 1) = Q^*(s, a)$ for all $(s, a) \in \mathcal{S} \times \mathcal{A}$ (Corollary A.1), i.e., by fixing the persistence to $k = 1$ we retrieve the optimal Q -function in the original MDP, and consequently, we can reconstruct a greedy optimal policy. This highlights that the primitive action space leads to the same optimal Q -function as with persistence options. Persistence, nevertheless, is helpful for exploration and learning, but for an optimal persistent policy ψ^* , there exists a primitive policy π^* with the same performance.

5 Persistent Q -learning

It may not be immediately clear what are the advantages of $\mathcal{H}_{\bar{k}}$ over traditional updates. These become apparent with its empirical counterpart $\widehat{\mathcal{H}}_{\bar{k}} = \mathbb{1}_{k \leq \bar{k}} \widehat{T}_{\bar{k}}^* + \mathbb{1}_{k > \bar{k}} \widehat{T}_{\bar{k}}^{\bar{k}}$, where:

$$(\widehat{T}_{\bar{k}}^* Q)(s_t, a_t, k) = r_{t+1}^k + \gamma^k \max_{(a', k') \in \mathcal{O}} Q(s_{t+k}, a', k'),$$

$$(\widehat{T}_{\bar{k}}^{\bar{k}} Q)(s_t, a_t, k) = r_{t+1}^{\bar{k}} + \gamma^{\bar{k}} Q(s_{t+k}, a_t, k - \bar{k}).$$

These empirical operators depend on the current partial history, which we define as: $H_t^{\bar{k}} := (s_t, a_t, r_{t+1}, s_{t+1}, r_{t+2}, \dots, s_{t+\bar{k}})$, used by Algorithm 1 to update each persistence in a backward fashion, as illustrated also in Appendix B. At timestep t , given a sampling persistence \bar{k}_t , for all sub-transitions of $H_t^{\bar{k}}$, starting at $t + i$ and ending in $t + j$, we apply $\widehat{\mathcal{H}}_t^{j-i}$ to $Q(s_{t+i}, a_t, k + d)$, for all $d \leq K_{\max} - k$, where $k = j - i$.

Algorithm 3: Multiple Replay Buffer Storing

Require: Maximum persistence K_{\max} , replay buffers $(\mathcal{D}_k)_{k=1}^{K_{\max}}$, transition tuple $(s_t, a_t, \bar{\kappa}_t, H_t^{\bar{\kappa}_t})$.

- 1: **for** $k = 1, \dots, K_{\max}$ **do**
- 2: **for** $\tau = 0, \dots, \max\{\bar{\kappa}_t - k, 0\}$ **do**
- 3: $\mathcal{D}_k \leftarrow \mathcal{D}_k \cup (s_{t+\tau}, a_t, s_{t+\tau+k}, r_{t+1+\tau}^k, k)$
- 4: **end for**
- 5: **for** $\tau = 1, \dots, \min\{\bar{\kappa}_t, k - 1\}$ **do**
- 6: $\mathcal{D}_k \leftarrow \mathcal{D}_k \cup (s_{t+\bar{\kappa}_t-\tau}, a_t, s_{t+\bar{\kappa}_t}, r_{t+1+\bar{\kappa}_t-\tau}^\tau, \tau)$
- 7: **end for**
- 8: **end for**

With these tools, it is possible to extend Q -learning (Watkins 1989) to obtain the Persistent Q -learning algorithm (abbreviated as Per Q -learning), described in Algorithm 2. The agent follows a policy $\psi_{\mathcal{O}}^{\epsilon}$, which is ϵ -greedy w.r.t. the option space and the current Q -function.

This approach extends the MSA- Q -learning (Schoknecht and Riedmiller 2003), by bootstrapping higher persistence action values from lower ones. More precisely, both methods apply the update related to \hat{T}^* , but MSA- Q -learning does not use $\hat{T}^{\bar{\kappa}}$ instead. As shown in the empirical analysis, in some domains this difference can be crucial to speed up the convergence. Similarly to MSA- Q -learning, we perform backwards updates to allow for an even faster propagation of values. The proposed approach also differs from TempoRL Q -learning (Biedenkapp et al. 2021), where action-persistence is selected using a dedicated value-function, learned separately from the Q -function. The asymptotic convergence of Persistent Q -learning to $Q_{\mathcal{K}}^*$ directly follows (Singh et al. 2000), being $\mathcal{H}^{\bar{\kappa}}$ a contraction and since their (mild) assumptions are satisfied.

6 Empirical Advantages of Persistence

In this section, we provide some numerical simulations to highlight the benefits of our approach. The settings are illustrative, to ease the detection of the individual advantages of persistence, before presenting more complex applications.

Exploration One of the main advantages of persistence is related to faster exploration, especially in goal-based environments (e.g., robotics and locomotion tasks). Indeed, persisting an action allows reaching faster states far from the starting point and, consequently, propagating faster the reward. The reason is due to the increased chances of 1-persistent policies to get stuck in specific regions. As explained in (Amin et al. 2021), persistence helps to achieve *self-avoiding* trajectories, by increasing the expected return time in previously visited states. Hence, we study the effects of a persisted exploratory policy on the MDP, i.e., a policy $\psi \in \Psi$ over persistence options \mathcal{O} (details in Appendix C).

To this purpose, we compute the *Kemeny’s constant* (Catral et al. 2010; Patel, Agharkar, and Bullo 2015), which corresponds to the expected first passage time from an arbitrary starting state s to another one s' under the stationary distribution induced by ψ . We consider four discrete tabular environments: *Open* is a 10x10 grid with no obstacles, while

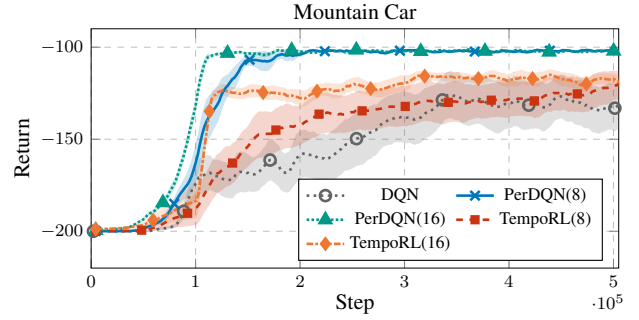


Figure 3: MountainCar results. Parenthesis in the legend denote K_{\max} . 20 runs (avg \pm 95% c.i.).

the others, presented in (Biedenkapp et al. 2021), are depicted in Figure 12. In Figure 1, we plot the variations of Kemeny’s constant as a function of the maximum persistence K_{\max} , while following a uniform policy ψ over \mathcal{O} . We observe that increasing K_{\max} promotes exploration, and highlights the different K_{\max} attaining the minimum value of the constant, due to the different complexity of the environments.

Sample Complexity The second relevant effect of persistence concerns with the sample complexity. The intuition behind persistence relies on the fact that the most relevant information propagates faster through the state-action space, thanks to multi-step updates. Moreover, these updates are associated to a lower discount factor, for which it is possible to obtain better convergence rates, as proved in (Metelli et al. 2020), in which the sample complexity in a k -persistent MDP is reduced by a factor $(1 - \gamma^k)/(1 - \gamma) > 1$. In order to evaluate the sample efficiency of Per Q -learning, separately from its effects on exploration, we considered a *synchronous* setting (Kearns and Singh 1999; Sidford et al. 2018) in a deterministic 6x6 Gridworld. At each iteration t , the agent has access to a set of independent samples for each state-action pair. In standard Q -learning, for each $(s, a) \in \mathcal{S} \times \mathcal{A}$, $Q(s, a)$ is updated. In Per Q -learning, the samples are combined to obtain each possible set of $\bar{\kappa}$ -persistent transitions, i.e., the tuples related to each possible $(s, a, k) \in \mathcal{S} \times \mathcal{O}$, with $K_{\max} = 6$; finally, the persistent Q function is updated.

In Figure 2 left, we compare the L_{∞} error of Q -learning estimating $Q^*(s, a)$, i.e., $\max_{s,a \in \mathcal{S} \times \mathcal{A}} |Q_t(s, a) - Q^*(s, a)|$, and that of Per Q -learning estimating $Q_{\mathcal{K}}^*(s, a, k)$, i.e., $\max_{s,a,k \in \mathcal{S} \times \mathcal{O}} |Q_t(s, a, k) - Q_{\mathcal{K}}^*(s, a, k)|$, as a function of the number of iterations t . We observe that, although estimating a higher-dimensional function (as $Q_{\mathcal{K}}^*(s, a, k)$ is a function of the persistence k too), Per Q -learning converges faster than Q -learning. In Figure 2 right, we plot the L_{∞} error experienced by Per Q -learning for the different persistence options $\mathcal{O}^{(k)}$, i.e., $\text{Error}_{\infty}(k) := \max_{s,a \in \mathcal{S} \times \mathcal{A}} |Q_t(s, a, k) - Q^*(s, a, k)|$ for $k \in \mathcal{K}$. As expected, higher values of k lead to faster convergence; consequently, the persistent Bellman operator helps improving the estimations also for the lower option sets. Indeed, we can see that also $Q_t(\cdot, \cdot, 1)$, the primitive actions Q -function, converges faster than classic Q -learning (details in Appendix E).

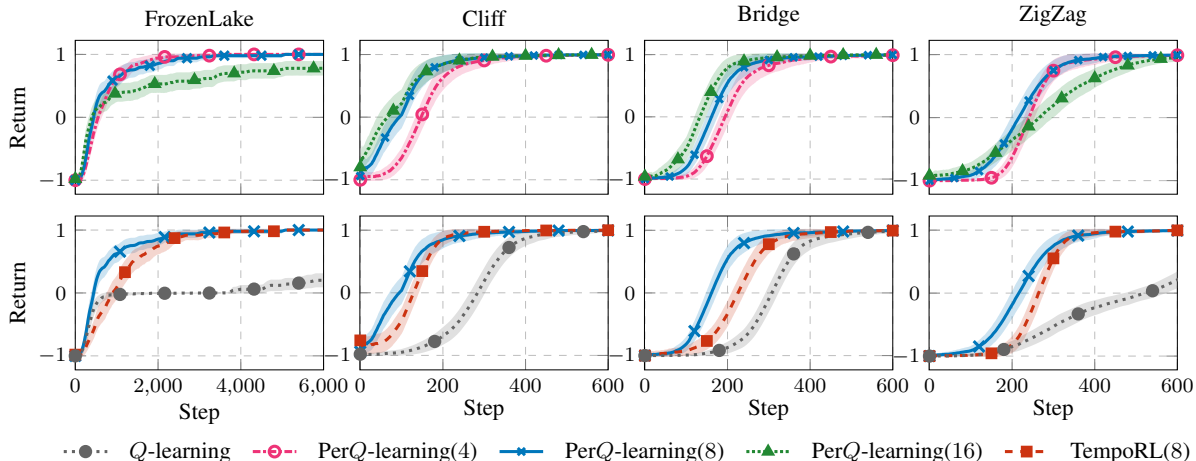


Figure 4: Results on tabular environments. Top row: performances with different maximum persistences. In the legend, parenthesis denote the selected K_{\max} . Bottom row: PerQ-learning and TempoRL comparison, $K_{\max} = 8$. 50 runs (avg \pm 95% c.i.).

7 Persistent Deep Networks

In this section, we develop the extension of PerQ-learning to high-dimensional settings. Deep RL methods are becoming of fundamental importance when learning on real systems, as well as the research of methods to improve exploration and learning speed. It is straightforward to exploit Deep Q-Networks (DQN (Mnih et al. 2013, 2015)) for learning in the options space \mathcal{O} . Standard DQN is augmented with K_{\max} distinct sets of action outputs, to represent Q-value of the options space $\mathcal{O} = \mathcal{A} \times \mathcal{K}$, while the first layers are shared, similarly to previous works (Arulkumaran et al. 2016; Lakshminarayanan, Sharma, and Ravindran 2017; Biedenkapp et al. 2021). The resulting algorithm, *Persistent Deep Q-Network* (PerDQN) is obtained by exploiting the application of the empirical all-persistence Bellman operator. The main differences between PerDQN and standard DQN consist in: (i) a modified ϵ -greedy strategy, which is equivalent to the one described for its tabular version; (ii) the use of *multiple* replay buffers accounting for persistence.

Persistence Replay Buffers Whenever an option $o_t = (a_t, \bar{k}_t)$ is executed, the partial history $H_t^{\bar{k}_t}$ is decomposed in all its sub-transitions, which are used to update Q-values at any persistence, as shown in Section 5. The sub-transitions are stored in multiple replay buffers \mathcal{D}_k , one for each persistence $k \in \mathcal{K}$. Specifically, \mathcal{D}_k stores tuples in the form (s, a_t, s', r, \bar{k}) , as summarized in Algorithm 3, where s and s' are the first and the last state of the sub-transition, r is the \bar{k} -persistent reward, and \bar{k} is the true length of the sub-transition, which will then be used to suitably apply $\widehat{H}_t^{\bar{k}}$.

Finally, the gradient update is computed by sampling a mini-batch of experience tuples from each replay buffer \mathcal{D}_k , in equal proportion. Given the current network and target parametrizations θ and θ^- , the temporal difference error of a sample (s, a, r, s', \bar{k}) is computed as $\widehat{H}_t^{\bar{k}} Q_{\theta^-}(s, a, k) - Q_{\theta}(s, a, k)$. Our approach differs from TempoRL DQN (Biedenkapp et al. 2021), which uses a dedicated network

to learn the persistence at each state and employs a standard replay buffer, ignoring the persistence at which samples have been collected.

8 Experimental Evaluation

In this section, we show the empirical analysis of our approach on both the tabular setting (PerQ-learning) and the function approximation one (PerDQN).

PerQ-learning We present the results on the experiments in tabular environments, particularly suited for testing PerQ-learning because of the sparsity of rewards. We start with the deterministic 6x10 grid-worlds introduced by Biedenkapp et al. 2021. In these environments, the episode ends if either the goal or a hole is reached, with +1 or -1 points respectively. In all the other cases, the reward is 0, and the episode continues (details in Appendix F.1). Moreover, we experiment the 16x16 FrozenLake, from OpenAI Gym benchmark (Brockman et al. 2016), with rewards and transition process analogous to the previous case, but with randomly generated holes at the beginning of the episode. The results are shown in Figure 4. In the top row, we compare the results on the performance when applying PerQ-learning with different $K_{\max} \in \{4, 8, 16\}$. We can detect a faster convergence when passing from $K_{\max} = 4$ to 8. However, the largest value of K_{\max} is not always the best one: while Bridge and Cliff show a slight improvement, performances in ZigZag and FrozenLake degrade. This is probably due to the nature of the environment. When there are many obstacles, high persistences might be inefficient, as the agent can get stuck or reach holes more easily. In the bottom plots of Figure 4 we selected the results with $K_{\max} = 8$, and compared them with TempoRL (with the same maximum *skip-length* $J = 8$) and classic Q-learning. In all cases, PerQ-learning outperforms the other methods, especially Q-learning, whose convergence is significantly slower. exploration is very small. With this maximum persistence value PerQ-learning outperforms TempoRL. Further experiments with different values

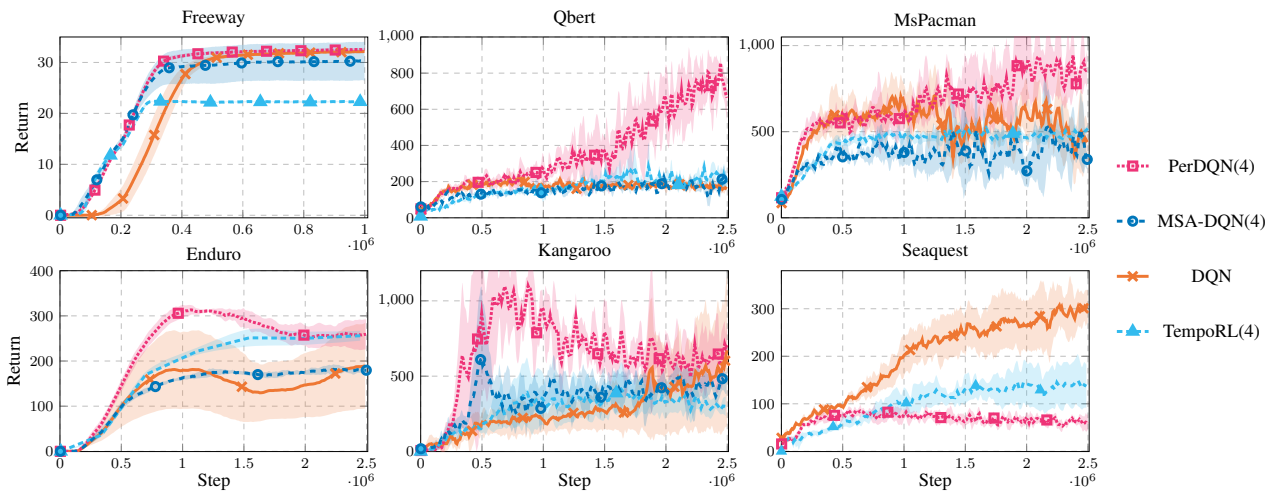


Figure 5: Atari games results. Parenthesis in the legend denote the maximum persistence K_{\max} . 5 runs (avg \pm 95% c.i.).

of K_{\max} have been reported in Appendix G.1, for space constraints. In general, PerQ-learning shows faster rates of improvements than TempoRL, especially in the first learning iterations. However, this advantage may not be consistent for every value of K_{\max} , and every environment, as also shown in Appendix G.1.

PerDQN Our implementation of PerDQN is based on OpenAI Gym (Brockman et al. 2016) and Baselines (Dhariwal et al. 2017) Python toolkits. We start with MountainCar (Moore 1991), as it is perhaps the most suited to evaluate the performance of persistence options. As shown in (Metelli et al. 2020), 1-step explorative policies usually fail to reach the goal. Figure 3 shows that TempoRL and DQN cannot converge to the optimal policy, as already noticed in (Biedenkapp et al. 2021), while PerDQN attains the optimal solution, that reaches the top of the mountain with the minimum loss.

The algorithm is then tested in the challenging framework of Atari 2600 games, where we want to validate that action persistence is beneficial to speed up the initial phases of learning also in large environments.

The same architecture from (Mnih et al. 2013), suitably modified as in Section 7, is used for all environments. For a fair comparison with TempoRL and standard DQN, persistence is implemented on top of the *frame skip*. Thus, a one-step transition corresponds to 4 frame skips. In Figure 5 we compare PerDQN with TempoRL and classic DQN. In five games out of six, our PerDQN displays a faster learning curve thanks to its ability of reusing experience, although in some cases (e.g. Kangaroo) PerDQN seems to inherit the same instability issues of DQN, we conjecture due to the overestimation bias (van Hasselt, Guez, and Silver 2016). In order to better understand which beneficial effects are provided by action persistence alone and which ones derive from the use of bootstrap operator, we run an ablation experiment on the same tasks removing the latter one. The resulting algorithm is then similar to the Deep RL version of MSA-Q-learning (Schoknecht and Riedmiller 2003), which we called MSA-DQN. The results show that PerDQN always dominates over

its counterpart without bootstrap. The crucial importance of the bootstrap operator is confirmed also in the MountainCar setting where removing this feature causes a performance decrease, making its score comparable to TempoRL (see Appendix G.2). Finally, we notice that in Seaquest persistence seems to be detrimental for learning, as DQN clearly outperforms PerDQN. In this task, agents have to choose either to move or to shoot some moving targets. Persisting the shooting action, thus, may force the agent to stay still for a long time, hitting nothing. A possible solution could consist in the introduction of *interrupting persistence*, in a similar fashion to interrupting options (Sutton, Precup, and Singh 1999; Mankowitz, Mann, and Mannor 2014), which is an interesting future research direction.

9 Discussion and Conclusions

In this paper, we considered RL policies that implement action persistence, modeled as *persistence options*, selecting a primitive action and its duration. We defined the *all-persistence* Bellman operator, which allows for an effective use of the experience collected at any time scale, as action-value function estimates can be updated simultaneously on the whole persistence set. In particular, low persistences (and primitive actions) can be updated by splitting the samples in their sub-transitions; high persistences can instead be improved by *bootstrap*, i.e. by estimating the partial missing information. After proving that the new operator is a contraction, we extended classic Q-learning and DQN to their persistent version. The empirical analysis underlines the benefits of the new operator for exploration and estimation. Furthermore, the experimental campaign on tabular and deep RL settings demonstrated the effectiveness of our approach and the importance of considering temporal extended actions, as well as some limitations. Future research directions include the introduction of persistence interruption and techniques to overcome the overestimation bias. Furthermore, one could investigate the use of the operator in the actor-critic framework to cope with continuous actions.

References

- Amin, S.; Gomrokchi, M.; Aboutalebi, H.; Satija, H.; and Precup, D. 2021. Locally Persistent Exploration in Continuous Control Tasks with Sparse Rewards. In *International Conference on Machine Learning*, 275–285. PMLR.
- Arulkumaran, K.; Dilokthanakul, N.; Shanahan, M.; and Bharath, A. A. 2016. Classifying options for deep reinforcement learning. *arXiv preprint arXiv:1604.08153*.
- Baird, L. C. 1994. Reinforcement learning in continuous time: Advantage updating. In *Proceedings of 1994 IEEE International Conference on Neural Networks (ICNN'94)*, volume 4, 2448–2453. IEEE.
- Bellemare, M. G.; Naddaf, Y.; Veness, J.; and Bowling, M. 2013. The arcade learning environment: An evaluation platform for general agents. *Journal of Artificial Intelligence Research*, 47: 253–279.
- Bertsekas, D.; and Shreve, S. E. 1996. *Stochastic optimal control: the discrete-time case*, volume 5. Athena Scientific.
- Biedenkapp, A.; Rajan, R.; Hutter, F.; and Lindauer, M. T. 2021. TempoRL: Learning When to Act. In *ICML*.
- Braylan, A.; Hollenbeck, M.; Meyerson, E.; and Mikkulainen, R. 2015. Frame skip is a powerful parameter for learning to play atari. In *Workshops at the Twenty-Ninth AAAI Conference on Artificial Intelligence*.
- Brockman, G.; Cheung, V.; Pettersson, L.; Schneider, J.; Schulman, J.; Tang, J.; and Zaremba, W. 2016. Openai gym. *arXiv preprint arXiv:1606.01540*.
- Catral, M.; Kirkland, S. J.; Neumann, M.; and Sze, N.-S. 2010. The Kemeny constant for finite homogeneous ergodic Markov chains. *Journal of Scientific Computing*, 45(1): 151–166.
- Dabney, W.; Ostrovski, G.; and Barreto, A. 2020. Temporally-Extended ϵ -Greedy Exploration. In *International Conference on Learning Representations (ICLR)*.
- Dhariwal, P.; Hesse, C.; Klimov, O.; Nichol, A.; Plappert, M.; Radford, A.; Schulman, J.; Sidor, S.; Wu, Y.; and Zhokhov, P. 2017. OpenAI Baselines. <https://github.com/openai/baselines>.
- G. Bellemare, M.; Ostrovski, G.; Guez, A.; Thomas, P.; and Munos, R. 2016. Increasing the Action Gap: New Operators for Reinforcement Learning. *Proceedings of the AAAI Conference on Artificial Intelligence*, 30(1).
- Grigsby, J.; Yoo, J. Y.; and Qi, Y. 2021. Towards Automatic Actor-Critic Solutions to Continuous Control. In *Deep RL Workshop NeurIPS 2021*.
- Gu, S.; Holly, E.; Lillicrap, T.; and Levine, S. 2017. Deep reinforcement learning for robotic manipulation with asynchronous off-policy updates. In *2017 IEEE international conference on robotics and automation (ICRA)*, 3389–3396. IEEE.
- Haarnoja, T.; Ha, S.; Zhou, A.; Tan, J.; Tucker, G.; and Levine, S. 2019. Learning to Walk Via Deep Reinforcement Learning. In Bicchì, A.; Kress-Gazit, H.; and Hutchinson, S., eds., *Robotics: Science and Systems XV*.
- Kalyanakrishnan, S.; Aravindan, S.; Bagdawat, V.; Bhatt, V.; Goka, H.; Gupta, A.; Krishna, K.; and Piratla, V. 2021. An Analysis of Frame-skipping in Reinforcement Learning. *arXiv preprint arXiv:2102.03718*.
- Kearns, M.; and Singh, S. 1999. Finite-sample convergence rates for Q-learning and indirect algorithms. *Advances in Neural Information Processing Systems (NIPS)*, 996–1002.
- Khan, A.; Feng, J.; Liu, S.; and Asghar, M. Z. 2019. Optimal skipping rates: training agents with fine-grained control using deep reinforcement learning. *Journal of Robotics*, 2019.
- Kilinc, O.; Hu, Y.; and Montana, G. 2019. Reinforcement Learning for Robotic Manipulation using Simulated Locomotion Demonstrations. *CoRR*, abs/1910.07294.
- Kiran, B. R.; Sobh, I.; Talpaert, V.; Mannion, P.; Al Sallab, A. A.; Yogamani, S.; and Pérez, P. 2021. Deep reinforcement learning for autonomous driving: A survey. *IEEE Transactions on Intelligent Transportation Systems*.
- Kirkland, S. 2010. Fastest expected time to mixing for a Markov chain on a directed graph. *Linear Algebra and its Applications*, 433(11-12): 1988–1996.
- Kober, J.; and Peters, J. 2014. *Learning Motor Skills - From Algorithms to Robot Experiments*, volume 97 of *Springer Tracts in Advanced Robotics*. Springer. ISBN 978-3-319-03193-4.
- Lakshminarayanan, A. S.; Sharma, S.; and Ravindran, B. 2017. Dynamic Action Repetition for Deep Reinforcement Learning. In Singh, S. P.; and Markovitch, S., eds., *Proceedings of the Thirty-First AAAI Conference on Artificial Intelligence (AAAI)*, 2133–2139. AAAI Press.
- Lillicrap, T. P.; Hunt, J. J.; Pritzel, A.; Heess, N.; Erez, T.; Tassa, Y.; Silver, D.; and Wierstra, D. 2016. Continuous control with deep reinforcement learning. In Bengio, Y.; and LeCun, Y., eds., *4th International Conference on Learning Representations (ICLR)*.
- Mankowitz, D. J.; Mann, T. A.; and Mannor, S. 2014. Time regularized interrupting options. In *International Conference on Machine Learning (ICML)*.
- Mann, T. A.; Mannor, S.; and Precup, D. 2015. Approximate Value Iteration with Temporally Extended Actions. *J. Artif. Intell. Res.*, 53: 375–438.
- Metelli, A. M.; Mazzolini, F.; Bisi, L.; Sabbioni, L.; and Restelli, M. 2020. Control frequency adaptation via action persistence in batch reinforcement learning. In *International Conference on Machine Learning (ICML)*, 6862–6873. PMLR.
- Metelli, A. M.; Mutti, M.; and Restelli, M. 2018. Configurable Markov Decision Processes. In Dy, J. G.; and Krause, A., eds., *Proceedings of the 35th International Conference on Machine Learning (ICML)*, volume 80 of *Proceedings of Machine Learning Research*, 3488–3497. PMLR.
- Mnih, V.; Kavukcuoglu, K.; Silver, D.; Graves, A.; Antonoglou, I.; Wierstra, D.; and Riedmiller, M. 2013. Playing atari with deep reinforcement learning. *arXiv preprint arXiv:1312.5602*.
- Mnih, V.; Kavukcuoglu, K.; Silver, D.; Rusu, A. A.; Veness, J.; Bellemare, M. G.; Graves, A.; Riedmiller, M.; Fiedjeland,

A. K.; Ostrovski, G.; et al. 2015. Human-level control through deep reinforcement learning. *nature*, 518(7540): 529–533.

Moore, A. W. 1991. Efficient memory based learning for robot control. *PhD Thesis, Computer Laboratory, University of Cambridge*.

Park, S.; Kim, J.; and Kim, G. 2021. Time Discretization-Invariant Safe Action Repetition for Policy Gradient Methods. *Advances in Neural Information Processing Systems (NeurIPS)*, 34.

Patel, R.; Agharkar, P.; and Bullo, F. 2015. Robotic surveillance and Markov chains with minimal weighted Kemeny constant. *IEEE Transactions on Automatic Control*, 60(12): 3156–3167.

Precup, D. 2001. *Temporal abstraction in reinforcement learning*. Ph.D. thesis, University of Massachusetts Amherst.

Puterman, M. L. 2014. *Markov Decision Processes: Discrete Stochastic Dynamic Programming*. John Wiley & Sons.

Schoknecht, R.; and Riedmiller, M. 2003. Reinforcement learning on explicitly specified time scales. *Neural Computing & Applications*, 12(2): 61–80.

Schulman, J.; Wolski, F.; Dhariwal, P.; Radford, A.; and Klimov, O. 2017. Proximal Policy Optimization Algorithms. *CoRR*, abs/1707.06347.

Sharma, S.; Srinivas, A.; and Ravindran, B. 2017. Learning to repeat: Fine grained action repetition for deep reinforcement learning. *arXiv preprint arXiv:1702.06054*.

Sidford, A.; Wang, M.; Wu, X.; Yang, L. F.; and Ye, Y. 2018. Near-optimal time and sample complexities for solving Markov decision processes with a generative model. In *Proceedings of the 32nd International Conference on Neural Information Processing Systems*, 5192–5202.

Singh, S.; Jaakkola, T.; Littman, M. L.; and Szepesvári, C. 2000. Convergence results for single-step on-policy reinforcement-learning algorithms. *Machine learning*, 38(3): 287–308.

Sutton, R. S.; and Barto, A. G. 2018. *Reinforcement learning: An introduction*. MIT press.

Sutton, R. S.; Precup, D.; and Singh, S. P. 1999. Between MDPs and Semi-MDPs: A Framework for Temporal Abstraction in Reinforcement Learning. *Artif. Intell.*, 112(1-2): 181–211.

Tallec, C.; Blier, L.; and Ollivier, Y. 2019. Making Deep Q-learning methods robust to time discretization. In Chaudhuri, K.; and Salakhutdinov, R., eds., *Proceedings of the 36th International Conference on Machine Learning (ICML)*, volume 97 of *Proceedings of Machine Learning Research*, 6096–6104. PMLR.

van Hasselt, H.; Guez, A.; and Silver, D. 2016. Deep Reinforcement Learning with Double Q-Learning. *Proceedings of the AAAI Conference on Artificial Intelligence*, 30(1).

Watkins, C. J. C. H. 1989. *Learning from delayed rewards*. Ph.D. thesis, King’s College, University of Cambridge.

Yu, H.; Xu, W.; and Zhang, H. 2021. TAAC: Temporally Abstract Actor-Critic for Continuous Control. *Advances in Neural Information Processing Systems (NeurIPS)*, 34.

A Proofs and Derivations

Lemma A.1 (Decomposition of r_k) Let $r_k(s, a)$ the expected k -persistent reward. Let $k' < k$, then it holds that:

$$r_k(s, a) = r_{k'}(s, a) + \gamma^{k'} \int_{\mathcal{S}} P_{k'}(ds' | s, a) r_{k-k'}(s', a) \quad \forall (s, a) \in \mathcal{S} \times \mathcal{A}.$$

Proof From the definition of r_k , it holds that $r_k(s, a) = \sum_{i=0}^{k-1} \gamma^i ((P^\delta)^i r)(s, a)$. Hence:

$$\begin{aligned} r_k(s, a) &= \sum_{i=0}^{k-1} \gamma^i ((P^\delta)^i r)(s, a) \\ &= \sum_{i=0}^{k'-1} \gamma^i ((P^\delta)^i r)(s, a) + \sum_{i=k'}^{k-1} \gamma^i ((P^\delta)^i r)(s, a) \\ &= r_{k'}(s, a) + \sum_{i=k'}^{k-1} \gamma^i \int_{\mathcal{S}} P_i(ds' | s, a) r(s', a) \\ &= r_{k'}(s, a) + \sum_{i=k'}^{k-1} \gamma^i \int_{\mathcal{S}} P_{k'}(ds'' | s, a) \int_{\mathcal{S}} P_{i-k'}(ds' | s'', a) r(s', a) \\ &= r_{k'}(s, a) + \gamma^{k'} \int_{\mathcal{S}} P_{k'}(ds'' | s, a) \sum_{j=0}^{k-k'-1} \gamma^j \int_{\mathcal{S}} P_j(ds' | s'', a) r(s', a) \\ &= r_{k'}(s, a) + \gamma^{k'} \int_{\mathcal{S}} P_{k'}(ds'' | s, a) r_{k-k'}(s'', a). \end{aligned}$$

■

Theorem 4.1 The all-persistence Bellman operator $\mathcal{H}^{\bar{k}}$ fulfills the following properties:

1. $\mathcal{H}^{\bar{k}}$ is a γ -contraction in L_∞ norm;
2. $Q_{\mathcal{K}}^*$ is its unique fixed point;
3. $Q_{\mathcal{K}}^*$ is monotonic in k , i.e., for all $(s, a) \in \mathcal{S} \times \mathcal{A}$ if $k \leq k'$ then $Q_{\mathcal{K}}^*(s, a, k) \geq Q_{\mathcal{K}}^*(s, a, k')$.

Proof

(i) First, we prove the contraction property: we consider the L_∞ -norm applied to the state-action-persistence space $\mathcal{S} \times \mathcal{A} \times \mathcal{K}$:

$$\begin{aligned} \|\mathcal{H}^{\bar{k}} Q_1 - \mathcal{H}^{\bar{k}} Q_2\|_\infty &= \sup_{s, a, k \in \mathcal{S} \times \mathcal{A} \times \mathcal{K}} |\mathcal{H}^{\bar{k}} Q_1(s, a, k) - \mathcal{H}^{\bar{k}} Q_2(s, a, k)| \\ &= \sup_{s, a, k \in \mathcal{S} \times \mathcal{A} \times \mathcal{K}} \left| \mathbb{1}_{k \leq \bar{k}} ((T^* Q_1)(s, a, k) - (T^* Q_2)(s, a, k)) \right. \\ &\quad \left. + \mathbb{1}_{k > \bar{k}} ((T^{\bar{k}} Q_1)(s, a, k) - (T^{\bar{k}} Q_2)(s, a, k)) \right| \\ &= \sup_{s, a, k \in \mathcal{S} \times \mathcal{A} \times \mathcal{K}} \left| \gamma^k \mathbb{1}_{k \leq \bar{k}} \int_{\mathcal{S}} P_k(ds' | s, a) \left[\sup_{a', k' \in \mathcal{A} \times \mathcal{K}} Q_1(s', a', k') - \sup_{a', k' \in \mathcal{A} \times \mathcal{K}} Q_2(s', a', k') \right] \right. \\ &\quad \left. + \gamma^{\bar{k}} \mathbb{1}_{k > \bar{k}} \int_{\mathcal{S}} P_{\bar{k}}(ds' | s, a) [Q_1(s', a, k - \bar{k}) - Q_2(s', a, k - \bar{k})] \right| \\ &\leq \sup_{s, a, k \in \mathcal{S} \times \mathcal{A} \times \mathcal{K}} \left\{ \gamma^k \mathbb{1}_{k \leq \bar{k}} \int_{\mathcal{S}} P_k(ds' | s, a) \left| \sup_{a', k' \in \mathcal{A} \times \mathcal{K}} Q_1(s', a', k') - \sup_{a', k' \in \mathcal{A} \times \mathcal{K}} Q_2(s', a', k') \right| \right. \\ &\quad \left. + \gamma^{\bar{k}} \mathbb{1}_{k > \bar{k}} \int_{\mathcal{S}} P_{\bar{k}}(ds' | s, a) \left| Q_1(s', a, k - \bar{k}) - Q_2(s', a, k - \bar{k}) \right| \right\} \\ &\leq \sup_{s, a, k \in \mathcal{S} \times \mathcal{A} \times \mathcal{K}} \left\{ \gamma^k \mathbb{1}_{k \leq \bar{k}} \int_{\mathcal{S}} P_k(ds' | s, a) \sup_{\tilde{a}, \tilde{k} \in \mathcal{A} \times \mathcal{K}} \left| Q_1(s', \tilde{a}, \tilde{k}) - Q_2(s', \tilde{a}, \tilde{k}) \right| \right\} \end{aligned}$$

$$\begin{aligned}
& + \gamma^{\bar{k}} \mathbb{1}_{k > \bar{k}} \int_{\mathcal{S}} P_{\bar{k}}(ds' | s, a) \sup_{\tilde{s}, \tilde{a} \in \mathcal{A} \times \mathcal{K}} \left| Q_1(\tilde{s}, \tilde{a}, k - \bar{k}) - Q_2(\tilde{s}, \tilde{a}, k - \bar{k}) \right| \Big\} \\
\leq & \sup_{s, a, k \in \mathcal{S} \times \mathcal{A} \times \mathcal{K}} \left\{ \gamma^k \mathbb{1}_{k \leq \bar{k}} \int_{\mathcal{S}} P_k(ds' | s, a) \sup_{\tilde{s}, \tilde{a}, \tilde{k} \in \mathcal{S} \times \mathcal{A} \times \mathcal{K}} \left| Q_1(\tilde{s}, \tilde{a}, \tilde{k}) - Q_2(\tilde{s}, \tilde{a}, \tilde{k}) \right| \right. \\
& \left. + \gamma^{\bar{k}} \mathbb{1}_{k > \bar{k}} \int_{\mathcal{S}} P_{\bar{k}}(ds' | s, a) \sup_{\tilde{s}, \tilde{a}, \tilde{k} \in \mathcal{S} \times \mathcal{A} \times \mathcal{K}} \left| Q_1(\tilde{s}, \tilde{a}, \tilde{k}) - Q_2(\tilde{s}, \tilde{a}, \tilde{k}) \right| \right\} \\
\leq & \sup_{s, a, k \in \mathcal{S} \times \mathcal{A} \times \mathcal{K}} \left\{ \left(\gamma^k \mathbb{1}_{k \leq \bar{k}} + \gamma^{\bar{k}} \mathbb{1}_{k > \bar{k}} \right) \|Q_1 - Q_2\|_{\infty} \right\} \\
= & \|Q_1 - Q_2\|_{\infty} \sup_{k \in \mathcal{K}} \gamma^{\min\{k, \bar{k}\}} = \gamma \|Q_1 - Q_2\|_{\infty}.
\end{aligned}$$

(ii): Since the contraction property holds, and being $(\mathcal{S} \times \mathcal{A} \times \mathcal{K}, d_{\infty})$ a complete metric space (with d_{∞} being the distance induced by L_{∞} norm), the Banach Fixed-point theorem holds, guaranteeing convergence to a unique fixed point.

We now show that $Q_{\mathcal{K}}^*$ is a fixed point of T^* . We first need to define the extended Bellman expectation operators $T^{\psi} : \mathcal{B}(\mathcal{S} \times \mathcal{O}) \rightarrow \mathcal{B}(\mathcal{S} \times \mathcal{O})$ with $f \in \mathcal{B}(\mathcal{S} \times \mathcal{O})$ and $\psi \in \Psi$:²

$$\begin{aligned}
(T^{\psi} f)(s, a, k) &= r_k(s, a) + \gamma^k \int_{\mathcal{S}} P_k(ds' | s, a) V(s'), \\
V(s) &= \sum_{(a, k) \in \mathcal{O}} \psi(a, k | s) f(s, a, k)
\end{aligned}$$

As with standard Bellman operators, it trivially holds that $T^{\psi} Q^{\psi} = Q^{\psi} \forall \psi \in \Psi$. Thus, we can take into account the definition of value function V^{ψ} of a policy ψ and the standard Bellman Equations:

$$\begin{aligned}
Q^{\psi}(s, a, k) &= r_k(s, a) + \gamma^k \int_{\mathcal{S}} P_k(ds' | s, a) V^{\psi}(s') \\
V^{\psi}(s) &= \sum_{(a, k) \in \mathcal{O}} \psi(a, k | s) Q^{\psi}(s, a, k)
\end{aligned} \tag{1}$$

Following the same argument as in (Puterman 2014), it holds that the optimal operator T^* improves the action-value function, i.e. $T^* Q^{\psi} \geq Q^{\psi}$, and consequently $Q_{\mathcal{K}}^*$ is the (unique) fixed point for T^* , i.e., $T^* Q_{\mathcal{K}}^* = Q_{\mathcal{K}}^*$ by contraction mapping theorem.

Moreover, it holds that $T^{\bar{k}} Q^{\psi} = Q^{\psi}$:

$$\begin{aligned}
(T^{\bar{k}} Q^{\psi})(s, a, k) &= r_{\bar{k}}(s, a) + \gamma^{\bar{k}} \int_{\mathcal{S}} P_{\bar{k}}(ds' | s, a) Q^{\psi}(s', a, k - \bar{k}) \\
&= r_{\bar{k}}(s, a) + \gamma^{\bar{k}} \int_{\mathcal{S}} P_k(ds' | s, a) \left[r_{k - \bar{k}}(s', a) + \gamma^{k - \bar{k}} \int_{\mathcal{S}} P_{k - \bar{k}}(ds'' | s', a) V^{\psi}(s'') \right] \\
&= \underbrace{r_{\bar{k}}(s, a) + \gamma^{\bar{k}} \int_{\mathcal{S}} P_k(ds' | s, a) r_{k - \bar{k}}(s', a)}_{r_k(s, a)} + \gamma^k \int_{\mathcal{S}} P_{\bar{k}}(ds' | s, a) \int_{\mathcal{S}} P_{k - \bar{k}}(ds'' | s', a) V^{\psi}(s'') \\
&= r_k(s, a) + \gamma^k \int_{\mathcal{S}} P_k(ds' | s, a) V^{\psi}(s') = Q^{\psi}(s, a, k),
\end{aligned} \tag{2}$$

where in Equation (2) we used Lemma A.1.

In conclusion,

$$\begin{aligned}
\mathcal{H}^{\bar{k}} Q_{\mathcal{K}}^* &= \left(\mathbb{1}_{k \leq \bar{k}} T^* + \mathbb{1}_{k > \bar{k}} T^{\bar{k}} \right) Q_{\mathcal{K}}^* \\
&= \mathbb{1}_{k \leq \bar{k}} T^* Q_{\mathcal{K}}^* + \mathbb{1}_{k > \bar{k}} T^{\bar{k}} Q_{\mathcal{K}}^* \\
&= \mathbb{1}_{k \leq \bar{k}} Q_{\mathcal{K}}^* + \mathbb{1}_{k > \bar{k}} Q_{\mathcal{K}}^* = Q_{\mathcal{K}}^*.
\end{aligned}$$

²The following can be extended without loss of generality to a continuous action space.

(iii) We provide the proof of monotonic property: given $(s, a) \in \mathcal{S} \times \mathcal{A}$, and given $k \leq k'$, we have:

$$\begin{aligned}
Q_{\mathcal{K}}^*(s, a, k) &= (T^* Q_{\mathcal{K}}^*)(s, a, k) \\
&= r_k(s, a) + \gamma^k \int_{\mathcal{S}} P_k(ds'|s, a) \max_{\bar{a}, \bar{k} \in \mathcal{A} \times \mathcal{K}} Q_{\mathcal{K}}^*(s', \bar{a}, \bar{k}) \\
&\geq r_k(s, a) + \gamma^k \int_{\mathcal{S}} P_k(ds'|s, a) Q_{\mathcal{K}}^*(s', a, k' - k) \\
&= T^k Q_{\mathcal{K}}^*(s, a, k') = Q_{\mathcal{K}}^*(s, a, k').
\end{aligned}$$

■

Corollary A.1 (Equivalence of $Q_{\mathcal{K}}^*$ and Q^*) For all $(s, a) \in \mathcal{S} \times \mathcal{A}$, the optimal action-value function Q^* and the optimal option-value function restricted to the primitive actions coincide, i.e.

$$Q_{\mathcal{K}}^*(s, a, 1) = Q^*(s, a)$$

Proof Trivially, $Q_{\mathcal{K}}^*$, defined on Ψ , coincides with the classic Q^* defined on the *primitive* policies $\pi \in \Pi$: in a first instance, we remark that $\Pi \subset \Psi$, hence all the policies defined on the space of primitive actions belong to the set of persistent policies. Furthermore, we can consider property (iii) of Theorem 4.1. As a consequence $Q_{\mathcal{K}}^*(s, a, 1) \geq Q^*(s, a, k) \forall k \in \mathcal{K}$, i.e., for each state $s \in \mathcal{S}$ there is at least one optimal primitive action $a \in \mathcal{A}$ which is optimal among all the option set \mathcal{O} . Consequently, the two optimal action-value functions coincide. ■

B Further clarifications

B.1 PerQ-learning Update scheme

In Figure 6 we present a scheme that shows an examples of the update order for Algorithm 2.

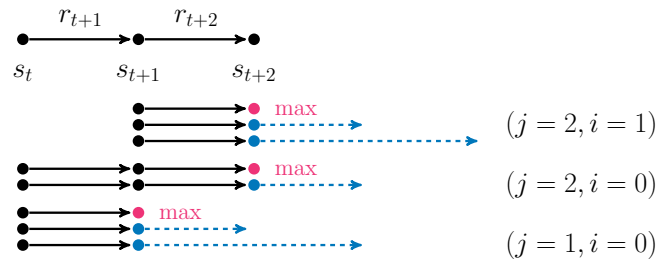


Figure 6: An example of the update order for Algorithm 1 with $\bar{K}_t = 2$ and $K_{\max} = 3$. Applications of \widehat{T}_t^* and $\widehat{T}_t^{K_t}$ are denoted, respectively, by magenta and blue nodes, while dashed arrows represent the bootstrap persistence.

C Details on Persistent Markov Chains and Kemeny constant

In this section, we provide more details regarding how to obtain the transition Kernel implied from a persistent random variable acting on the environment, and how to compute its Kemeny's constant.

Consider an agent where actions are sampled from a generic policy $\pi(\cdot|s) =: \pi$ on the action space \mathcal{A} , independent from the current state, and where persistence is sampled from a discrete distribution ω with support in $\{1, \dots, K_{\max}\}$, independent from π . They constitute the policy ψ over persistence options. The k -step Transition Chain induced by π over the state space \mathcal{S} is defined as $P_k^\pi(s'|s) = \int_{\mathcal{A}} P_k(s'|s, a)\pi(da|s)$. This is equivalent to the Markov chain induced by π in the k -step MDP, where the control frequency is set to k times the base duration δ . We now consider the transition probability induced by the joint probability distributions π and ω up to a maximum of K_{\max} steps, which for simplicity will here be referred as K . In order to define it, it is necessary to consider a fixed horizon H : when the total number of steps in the trajectory reaches the horizon, then the (eventual) persistence is stopped. This means that, if we start for example at the $H - j$ step, the probability of persisting j times the sampled action is equivalent to $\sum_{i \geq j} \omega_i$. This assumption is necessary for the Markov condition to hold. As a consequence, we define $\tilde{\omega}_j = \{\tilde{\omega}_{i,j}\}_i$ as a reduced distribution of ω to j steps:

$$\tilde{\omega}_{i,j} := \begin{cases} \omega_i & \text{if } i < j \\ \sum_{i=j}^K \omega_i & \text{otherwise} \end{cases}.$$

Finally we can recursively define the transition probability in H steps, induced by π and ω as:

$$\mathbb{P}_H^{\pi, \omega} := \sum_{k=1}^K \tilde{\omega}_{k, H \wedge K} \mathbb{P}_{H-k}^{\pi, \tilde{\omega}_{H-k}} P_k^\pi, \quad (3)$$

where $\mathbb{P}_0^{\pi, \omega} = \mathbb{1}_{\mathcal{S} \times \mathcal{S}}$ and $a \wedge b = \min\{a, b\}$. Equation (3) is not trivial and needs some clarifications. Let's consider an example, where $K = 4$ and $H = 3$. In this case the persistence distribution is $\omega = \{\omega_1, \omega_2, \omega_3, \omega_4\}$.

- With probability $\omega_3 + \omega_4$, the sampled persistence is equal to 3, and the related transition is P_3^π (since $H = 3$, sampling persistence 4 leads to repeat the action for 3 times);
- With probability ω_2 , the sampled persistence is equal to 2. The first two steps evolve as P_2^π , and the last step follows $\mathbb{P}_1^{\pi, \tilde{\omega}_1} = P^\pi$;
- With probability ω_1 , the action is selected only once, and at the next step it has to be sampled again and eventually persisted for two steps w.p. $\omega_2 + \omega_3 + \omega_4$.

In other terms, denoting $\tilde{\omega}_1 = \omega_1$, $\tilde{\omega}_2 = \omega_2$, and $\tilde{\omega}_3 = \omega_3 + \omega_4$:

$$\begin{aligned} \mathbb{P}_3^{\pi, \omega} &= \tilde{\omega}_3 P_3^\pi + \tilde{\omega}_2 P^\pi P_2^\pi + \tilde{\omega}_1 [\tilde{\omega}_1 P^\pi P^\pi + (\tilde{\omega}_2 + \tilde{\omega}_3) P_2^\pi] P^\pi \\ &= \tilde{\omega}_3 \mathbb{1} P_3^\pi + \tilde{\omega}_2 \underbrace{[(\tilde{\omega}_1 + \tilde{\omega}_2 + \tilde{\omega}_3) P^\pi]}_{=\mathbb{P}_1^{\pi, \tilde{\omega}_1}} P_2^\pi + \\ &\quad + \tilde{\omega}_1 \underbrace{[\tilde{\omega}_1 (\tilde{\omega}_1 + \tilde{\omega}_2 + \tilde{\omega}_3) P^\pi P^\pi + (\tilde{\omega}_1 + \tilde{\omega}_2) P_2^\pi]}_{=\mathbb{P}_2^{\pi, \tilde{\omega}_2}} P_1^\pi \\ &= \tilde{\omega}_3 \mathbb{P}_0^{\pi, \omega} P_3^\pi + \tilde{\omega}_2 \mathbb{P}_1^{\pi, \omega} P_2^\pi + \tilde{\omega}_1 \mathbb{P}_2^{\pi, \omega} P_1^\pi \end{aligned}$$

The meaning of the modified distribution $\tilde{\omega}$ is related to the fact that, once the trajectory evolved for k steps, the remaining $H - k$ are still sampled, but when the last step H is reached, then the agent stops repeating in any case.

Kemeny's constant computation The formula used to compute the Kemeny's constant from the transition Kernel $\mathbb{P}_H^{\pi, \omega}$ can be obtain thanks to the following Proposition (Kirkland 2010).

Proposition C.1 (Kemeny's constant of an irreducible Markov Chain) Consider a Markov chain with an irreducible transition matrix P with eigenvalues $\lambda_1 = 1$ and $\lambda_i, i \in \{2, \dots, n\}$. The Kemeny constant of the Markov chain is given by

$$Kem = \sum_{i=2}^n \frac{1}{1 - \lambda_i}.$$

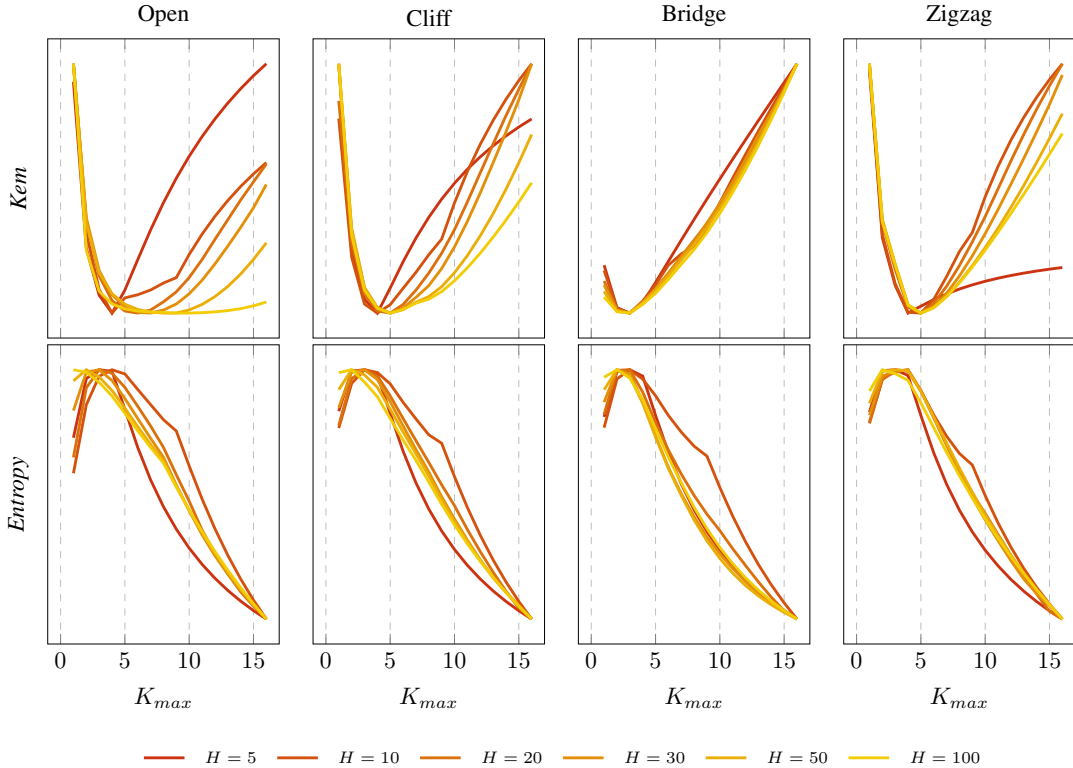


Figure 7: Normalized Kemeny’s constant and entropy in Tabular environments as function of the maximum persistence and horizon H .

The introduction of the parameter H is necessary to retrieve an irreducible transition matrix $\mathbb{P}_H^{\pi, \omega}$ maintaining the Markov property.

In order to compute the curves of Kemeny’s constant in Figure 1, we consider a K_{max} as a variable, and exploration is performed by a discrete uniform random variable in $\mathcal{O} = \bigcup_{k \in \mathcal{K}} \mathcal{O}^{(k)}$, i.e., the distribution π is uniform over the action space $\mathcal{A} = \{left, down, right, up\}$, and ω uniform over \mathcal{K} . In Figure 7 we show the curves of Kemeny’s constant and entropy with different value of K_{max} and H , and Figure 1 presented in Section 6 refers to the same Kemeny’s curves selected for $H = 30$.

As we can see in the figure, for each value of H there is a similar pattern: increasing K_{max} , the related values for Kemeny’s constant initially tend to decrease, indicating that persistence helps for a faster exploration through the state space. Persisting actions for long times does not help exploration, since agents might be more frequently standing in front of walls. Consequently, depending on the different design of the environments, Kemeny’s values begin to increase. In the bottom plots of Figure 7 we can observe also the curves related to the entropy induced by $\mathbb{P}_H^{\pi, \omega}$: again, the maximum value of entropy is attained by $K_{max} > 1$. However, the curves soon start to decrease dramatically, indicating that reaching distant states sooner is not strictly related to its visitation frequency.

D Further Exploration Advantages: MountainCar

In this section, we provide further evidence regarding the advantages of exploration. We study the effects of a persisted random policy on the MDP, i.e., a policy $\psi \in \Psi$ over persistence options \mathcal{O} in Mountain Car. We have collected all the states traversed by a full random agent with different values of K_{max} , both with a fixed persistence (Figure 8) and a dynamic persistence (Figure 9). The figures represent heatmaps of the visitation frequency in the state space. As we can see, when K_{max} is low the agent has less chance to reach the goal (represented by the blue dotted line). Increasing the persistence, the distribution over the states starts covering a wider region of the state space and reaching the goal with higher probability.

We can observe that, even if the goal for some values of K is almost equally visited, with a fixed persistence we have a different distribution of visited states. Moreover, a fixed, high persistence does not provide sufficient exploration to reach the goal, as we can see in figure 8 with $K = 64$, especially if compared to the dynamic version in figure 9.

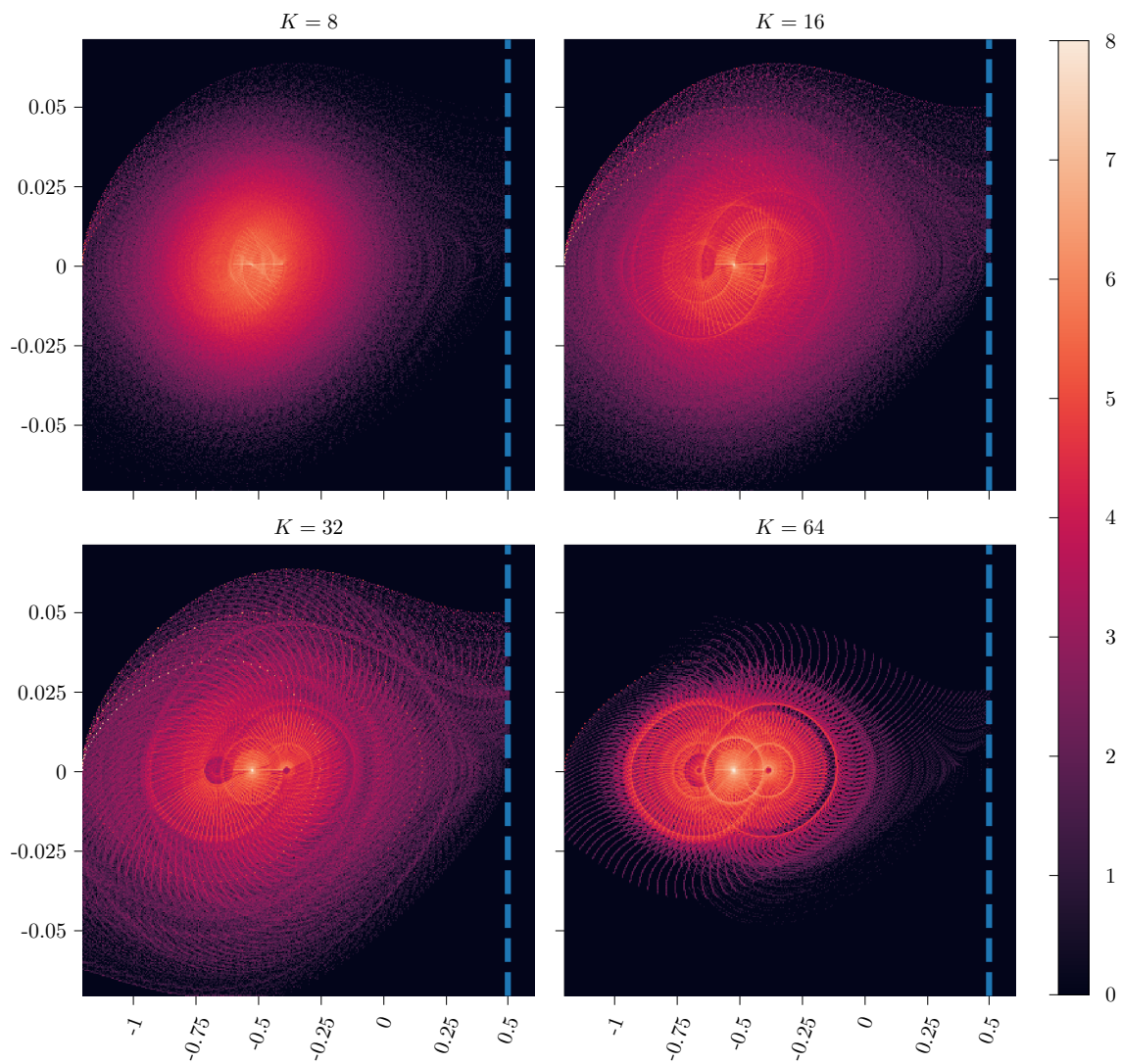


Figure 8: Visitation frequencies in Mountain Car environment of different random policies with fixed K persistences. The value represents in a logarithmic scale the counter of visited states. The x and y axes are respectively the position and the velocity of the car. Blue dotted line represents the goal. 10.000 episodes

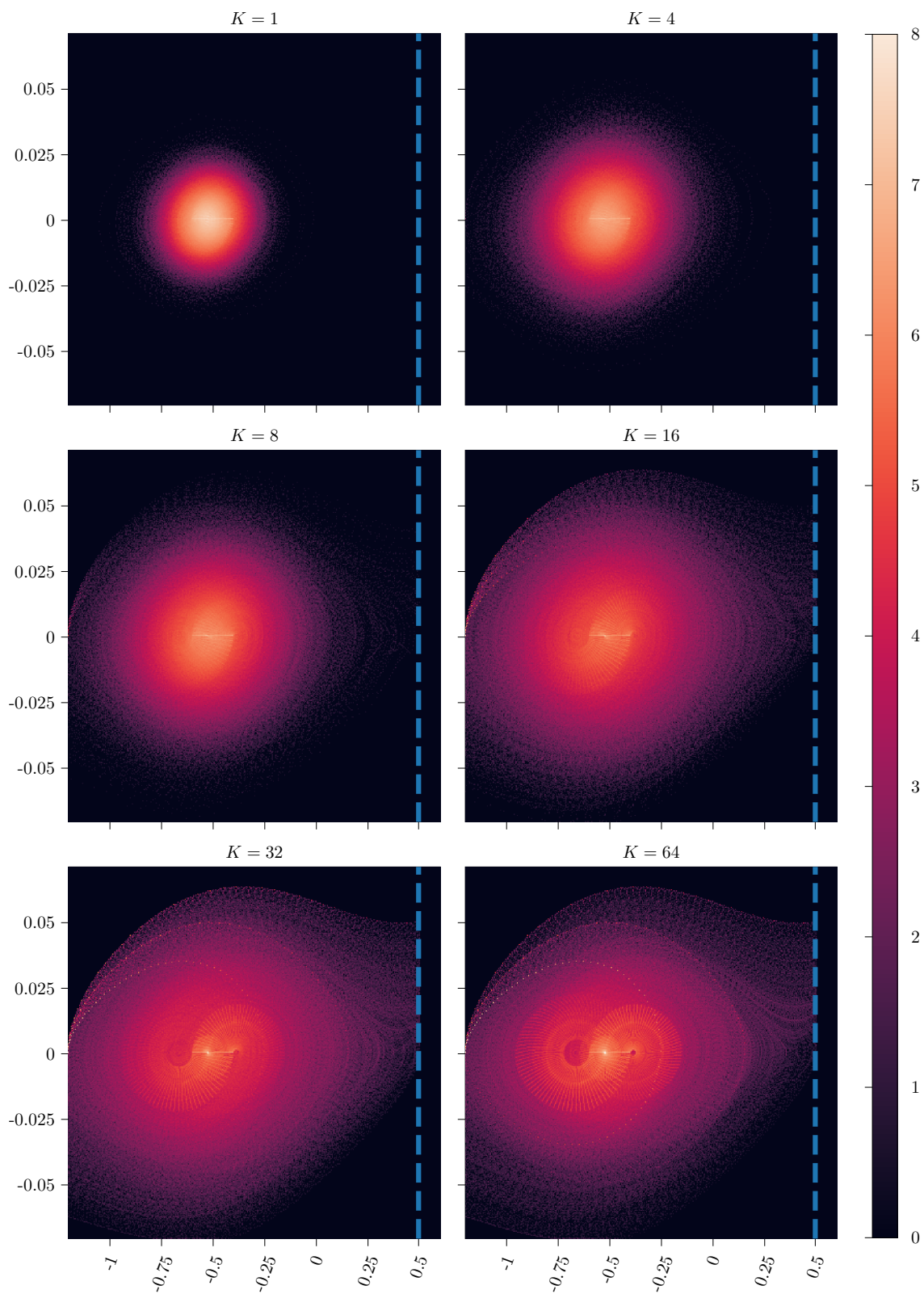


Figure 9: Visitation frequencies in Mountain Car environment of different random persistence options. The value represents in a logarithmic scale the counter of visited states. The x and y axes are respectively the position and the velocity of the car. Blue dotted line represents the goal. 10.000 episodes

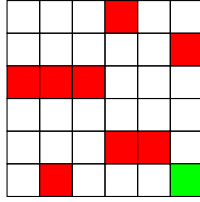


Figure 10: Grid environment. Red cell denote holes, green cells the goal.

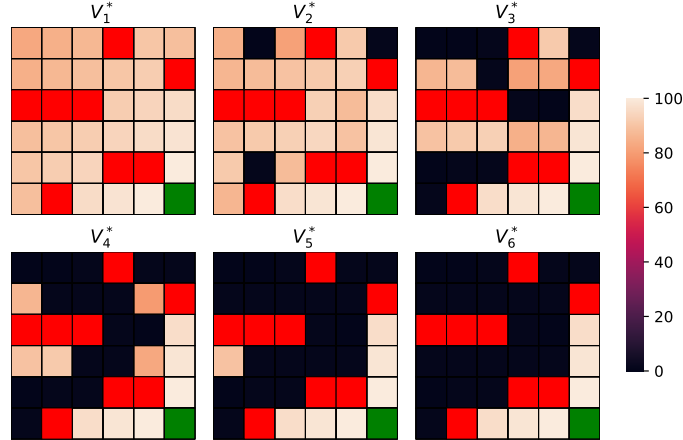


Figure 11: k -value function representation for different persistence values k ($K_{\max} = 6$). Red cells denote holes, green cell the goal.

E Synchronous Update: additional Results

In this appendix, we report some additional information related to the experiments with synchronous PerQ-learning updates shown in Section 6.

The environment considered is depicted in Figure 10: a 6x6 deterministic gridworld, with holes. The set of (primitive) actions is $\mathcal{A} = \{left, down, right, up\}$. Transitions are deterministic. Going outside the borders and falling off a hole result in a punishment with a negative reward, respectively equal to -100 and -10 (hence, outer borders are not blocking the movement of the agent). The reward for reaching the goal instead is equal to +100. In all these cases the episode terminates; all other states result in a small negative reward (-1), to incentivize finding the shortest paths towards the goal.

In order to exploit only the convergence properties of PerQ-learning algorithm, without considering the exploration factor, we consider a synchronous learning framework: we assume to have access to the whole transition model, in such that, at each iteration t , we are able to collect an independent sample $s' \sim P(\cdot|s, a)$ for every state-action pair $(s, a) \in \mathcal{S} \times \mathcal{A}$. Since the environment is deterministic, this means that we have access to the whole transition matrix P . For each simulation, the value estimation for each state-action pair (or state-option pair, in the case of PerQ-learning) is initialized sampling from a standard gaussian random variable. In each iteration of Q-learning, the algorithm performs a full update of the Q-function estimates. In each iteration of PerQ-learning, before performing the full update, the *primitive* tuples are combined together, in order to collect a sample for each possible (s, a, k) pair in $\mathcal{S} \times \mathcal{A} \times \mathcal{K}$.

In the plots on Figure 2, we represented the overall convergence to Q^* and the convergence of the $Q_{\mathcal{K}}$ -value function restricted on the k -persistent actions $\mathcal{O}^{(k)}$, as specified in Section 6.

The representations of the k -step value functions V_k^* are shown in Figure 11, where $V_k^*(s) = \max_{a \in \mathcal{A}} Q^*(s, a, k)$. It is useful to remark that this value function do not coincide with the optimal value function in the k -persistent MDP \mathcal{M}_k , as $V_k^*(s)$ represent the value function at the state s restricted to persist k times only the first action, and the following the optimal policy π^* .

Parameters used for experiments:

- Initial estimation: $Q(s, a, k) \sim \mathcal{N}(0, 1) \forall (s, a, k) \in \mathcal{S} \times \mathcal{A} \times \mathcal{K}$;
- Discount factor: $\gamma = 0.99$;
- Learning rate: $\alpha = 0.1$;
- Maximum number of iterations: 400 (plots truncated at 200).

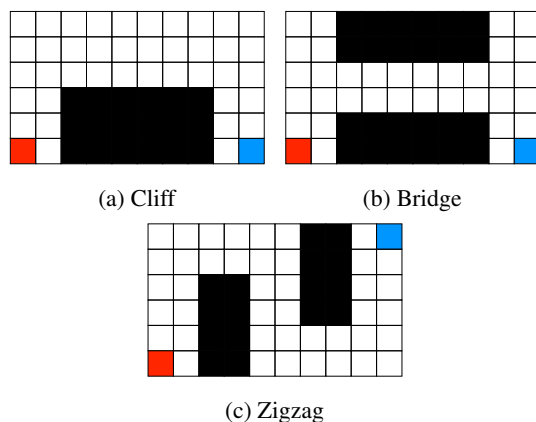


Figure 12: Tabular Gridworlds. Red cells denote the starting state and blue cells the goal state.

F Details on Experimental Evaluation

In this appendix, we report more details about our experimental framework. In Appendix F.1 we provide more details about Per Q -learning and the tabular setting; in Appendix F.2 and F.3 we focus on PerDQN and the deep RL experiments, respectively on Mountain Car and Atari games.

Infrastructure and computational times The experiments have been run on a machine with two GPUs: a Nvidia Tesla K40c and a Nvidia Titan Xp with a Intel(R) Core(TM) i5-4570 CPU @ 3.20GHz (4 cores, 4 thread, 6 MB cache) and 32 GB RAM.

Computational times for Atari experiments: a single run of Freeway, with our infrastructure, needs around 4 hours for DQN, 5h 20 min for PerDQ and TempoRL. The other Atari games require 10h for DQN, 12h for PerDQ and 13h 20min for TempoRL.

F.1 Tabular Environments

The first environments tested are the deterministic 6x10 grids shown in Figure 12 and presented in Biedenkapp et al. 2021. These environments are deterministic, and the outer borders block the agent from moving outside the grid (for example, an agent being at the top left cell will not move with an Up action). Falling in the holes (black cells in Figure 12) results in a -1 reward, while the goal is worth a positive reward, equal to $+1$. All other states have no reward. Reaching a Hole or the Goal terminates an episode.

Along with these three environments, we tested also the results on FrozenLake, available among OpenAi gym toolkit (Brockman et al. 2016). The transition process and the rewards are the same as in the previous case; the only differences are the bigger map (16x16) and the presence of random holes, such that each run is performed on a new map. For each new random map generated, the probability for each tile to be a hole (or frozen, according to the environment description) is equal to 0.85.

Parameters:

- Initial estimation: $Q(s, a, k) \sim \mathcal{N}(0, 1) \forall (s, a, k) \in \mathcal{S} \times \mathcal{A} \times \mathcal{K}$;
- Discount factor: $\gamma = 0.99$;
- Learning rate: $\alpha = 0.01$;
- Maximum number of iterations: 6000 for FrozenLake, otherwise 600;
- Random policy probability: Exponentially decreasing: $\epsilon_t = 0.99^t$.

F.2 Mountain Car

For Mountain Car experiments, the architecture chosen is a MLP: the first two hidden layers, consisting of 128 rectifier units, are shared among all persistences. The third hidden layer instead is diversified for each persistence value k , and each one is composed of 64 rectifier neurons and connected to three outputs, one for each action with its own persistence value.

The parameters adopted for the experiments are the following:

- Discount factor: $\gamma = 1$;
- Maximum number of iterations: 6×10^5 (truncated to 5×10^5 in the plots);
- Batch size: 32 for each persistent value;

- Replay buffer size: 50000 for each persistent value;
- Random policy probability: linearly decreasing, starting from $\epsilon_0 = 1$, to a final value $\epsilon_f = 0.01$, reached at 15% of the total number of iterations;
- Target update frequency: every 1000 steps;
- Train frequency: 1;
- Gradient clip: 10;
- Learning starts: 1000 (2000 only for Freeway);
- Loss function: Huber loss;
- Optimizer: Adam, with learning rate $\alpha = 10^{-4}$, $\beta_1 = 0.9$, $\beta_2 = 0.999$;
- Prioritized replay buffers, of size 5×10^4 fro each persistence value, and default prioritization coefficients $\alpha_p = 0.6$, $\beta_p = 0.4$;

F.3 Atari

For Atari games, the architecture chosen is based on that presented in (Mnih et al. 2015), with three convolutional layers. the first hidden layer takes as input an $84 \times 84 \times 4$ image and convolves 32 filters of 8×8 with stride 4, with the application of rectifier nonlinearities. The second has 32 input channels, 64 output channels, a kernel size of 4 and a stride of 2, again with ReLU activations, as well as the third convolutional layer, with kernel size of 3 and a stride of 1, and 64 output channels. The convolutional structured is shaerd among all persistences, while the fully-connected hidden layer, consisting of 128 rectifier units, is differentiated for each persistence value k . Each one of these layers is fully-connected with the output layer, with a single output for each possible action.

The OpenAi Gym environments used are in the *deterministic-v0* version (e.g. *FreewayDeterministic-v0*), which do not make merging operations among the 4 input frames, but consideres only the last one.

The parameters adopted are the following:

- Discount factor: $\gamma = 0.99$;
- Maximum number of iterations: 2.5×10^6 ;
- Batch size: 32 for each persistent value;
- Replay buffer size: 50000 for each persistent value;
- Random policy probability: linearly decreasing, starting from $\epsilon_0 = 1$, to a final value $\epsilon_f = 0.01$, reached at 17% of the total number of iterations;
- Target update frequency: every 500 steps;
- Train frequency: 1;
- Gradient clip: 10;
- Learning starts: 1000 (2000 only for Freeway);
- Loss function: Huber loss;
- Optimizer: Adam, with learning rate $\alpha = 5 \times 10^{-4}$, $\beta_1 = 0.9$, $\beta_2 = 0.999$;
- Prioritized replay buffers, of size 5×10^4 from each persistence value, and default prioritization coefficients $\alpha_p = 0.6$, $\beta_p = 0.4$.

G Additional Results

In this appendix, we report more experimental results.

G.1 Tabular environments

Here we consider the results related to the tabular environments. In Figure 13 we present the full comparison among PerQ-learning-learning and TempoRL. As said in Section 8, we can observe a general faster convergence of the former. However, TempoRL is more robust with higher persistences, as in complex environments such as ZigZag and FrozenLake the performance does not degrade as PerQ-learning learning.

Furthermore we analyzed the impact of the Bootstrap operator: as an ablation study, we performed the same PerQ-learning learning evaluation without this feature. As a result, we can see that the returns are dramatically worse. Often, they perform even worse than classic Q learning: the reason of this behavior is due to the fact that, if a certain persistence value k is not feasible for a state action pair (s, a) (because of the geometry of the environment), its related value estimation $Q(s, a, k)$ will never be updated, and the algorithm may keep choosing it as the best one among the others. In TempoRL, albeit the absence of a Bootstrap, the update of the *skip-value* function is instead updated by using the standard action-value function, improving the estimation.

G.2 PerDQN additional results

PerDQN with increased K_{max} in Atari games Here we investigate the effects of an increased value of K_{max} in Atari games: in Figure 15 we show the results obtained on Freeway, by increasing the maximum persistence to 8 for both TempoRL and PerDQN. The same $K_{max} = 8$ for PerDQN has been tested on the other Atari games, and shown in Figure 16 (we excluded Seaquest, as we have already shown that persistence in this environment is detrimental for learning. As we can see, an increased maximum persistence $K_{max} = 8$ does not provide improvements w.r.t. $K_{max} = 4$ for the majority of the environments. A slight improvement can be seen for Freeway, while TempoRL, albeit providing a better learning curve than the one obtained with skip size equal to 4, is still unable to converge to the optimal policy.

MountainCar, PerDQN without bootstrap Here we investigate the effects of the Bootstrap operator on PerDQN. In order to do so, we experimentally evaluated the algorithm without this feature on MountainCar and on the Atari games where persistence seemed to have beneficial effects (hence, with the exclusion of Seaquest environment). The results related to the Atari environments are shown in Figure 5, while MountainCar performances are shown in Figure 14: the version without bootstrap recalls the same contribution brought in (Schoknecht and Riedmiller 2003) with MSA-Q-learning, hence it is here denoted as MSA-DQN. As we can see, bootstrap is an essential feature for PerDQN to converge rapidly to the optimal policy and to be robust. Indeed, without the bootstrap, the performances are worse, similar to TempoRL, and their variance is dramatically higher.

G.3 PerQ-learning: computational times

We ran PerQ-learning on the tabular environments for different values of K_{max} keeping track of the training time. We fixed the number of collected trajectories, but the trajectories can be of different lengths since the environments are goal-based. In Figure 17, we observe that in all environments the minimum is attained by a value of $K_{max} > 1$. This means that the computational overhead due to using larger values of K_{max} is compensated by a faster learning speed, leading to shorter trajectories overall. Note that $K_{max} = 1$ corresponds to classic Q-learning.

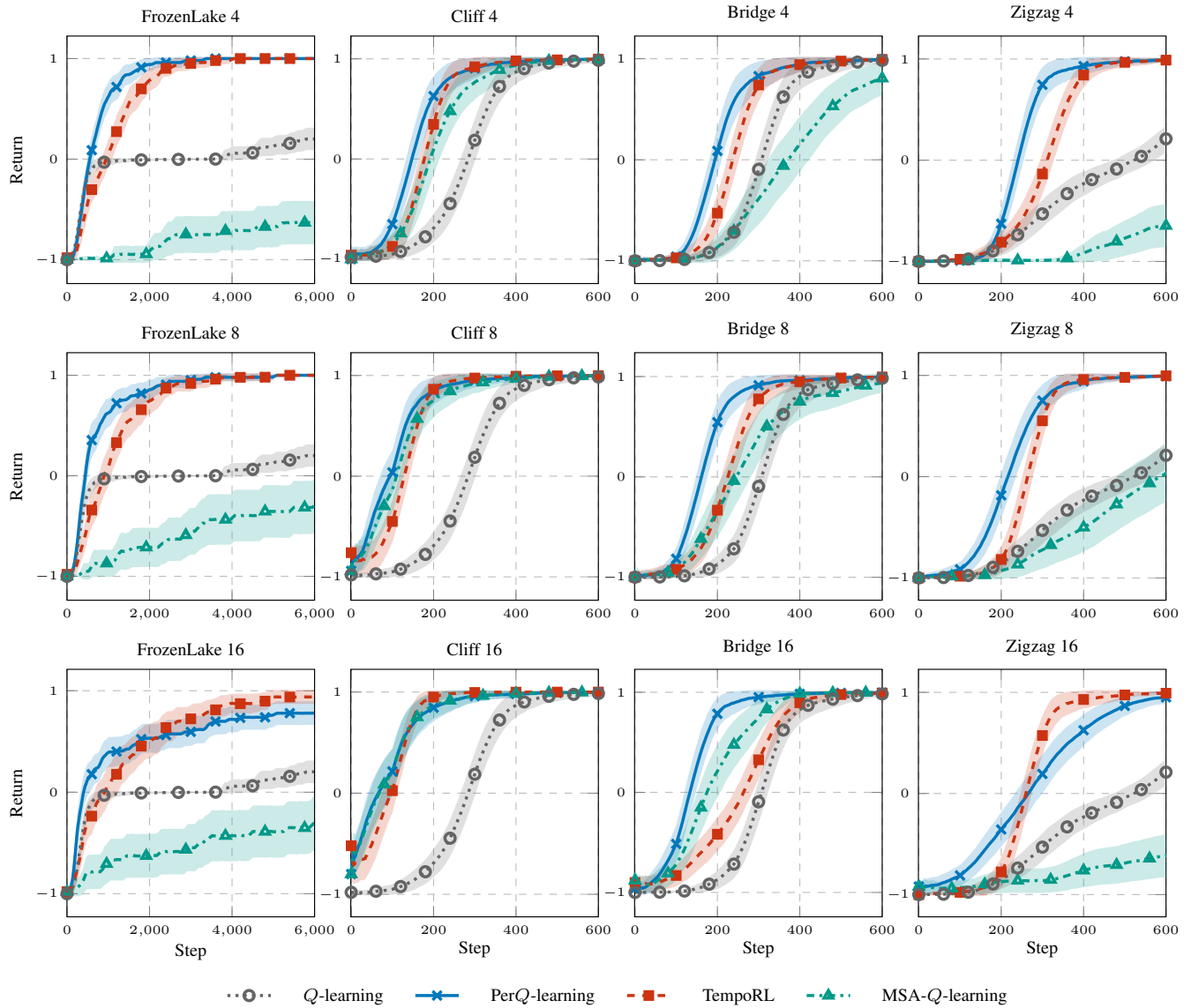


Figure 13: Results of Q -learning, TempoRL, Per Q -learning and MSA- Q -learning in different tabular environments and maximum persistences. On each row, a different maximum persistence is selected for both algorithms. 50 runs (avg \pm 95% c.i.).

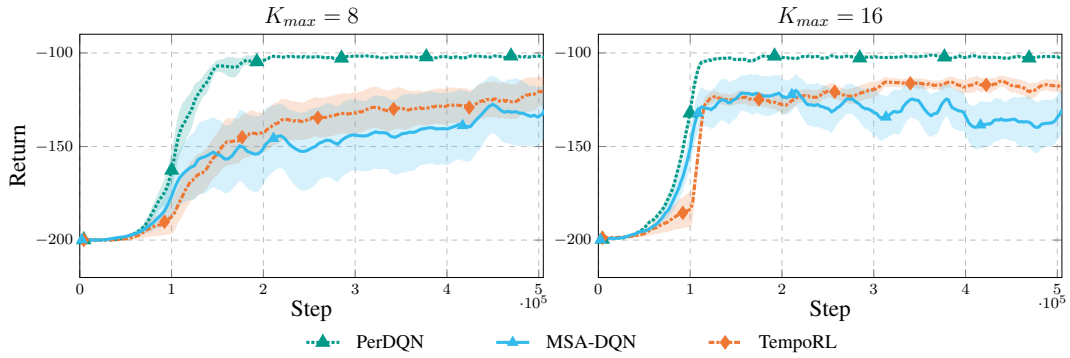


Figure 14: PerDQN additional results on MountainCar. Return comparison of PerDQN with and without bootstrap (MSA-DQN) and TempoRL. 20 runs (avg \pm 95% c.i.)

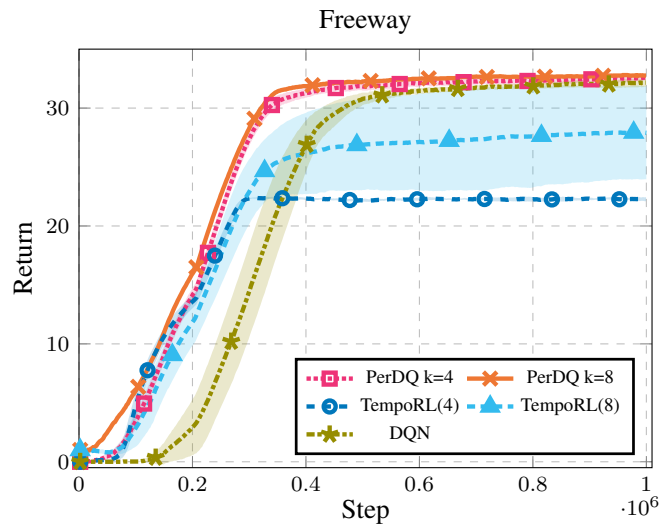


Figure 15: PerDQN additional results on Freeway. Return comparison of PerDQN and TempoRL with maximum persistence 4 and 8. Parenthesis denote the maximum persistence chosen. 5 runs (avg \pm 95% c.i.)

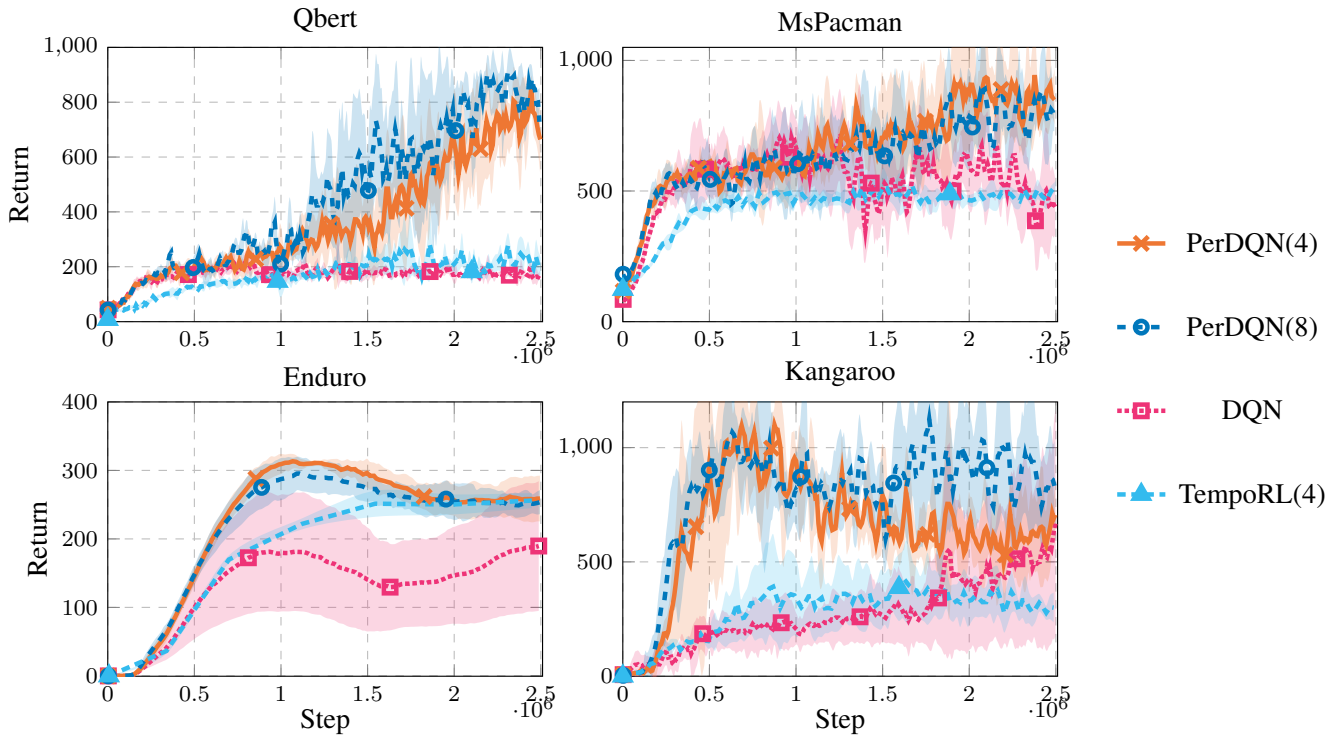


Figure 16: Atari games results for DQN and PerDQN, with $K_{max} = 4$ and 8 . 5 runs (avg \pm 95% c.i.).

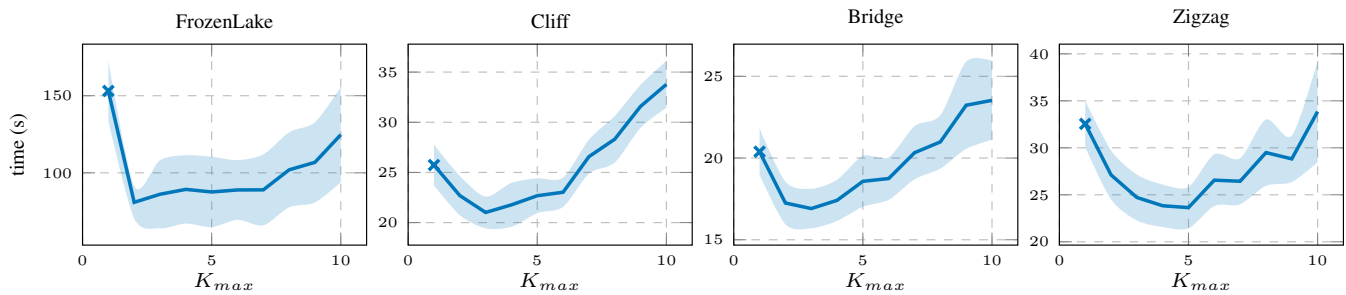


Figure 17: Computational times required for a complete run of PerQ-learning on tabular environments with different Maximum Persistences. 20 runs. avg \pm 95% c.i.

G.4 Experiments with the same number of updates and Comparison with ϵ -greedy exploration

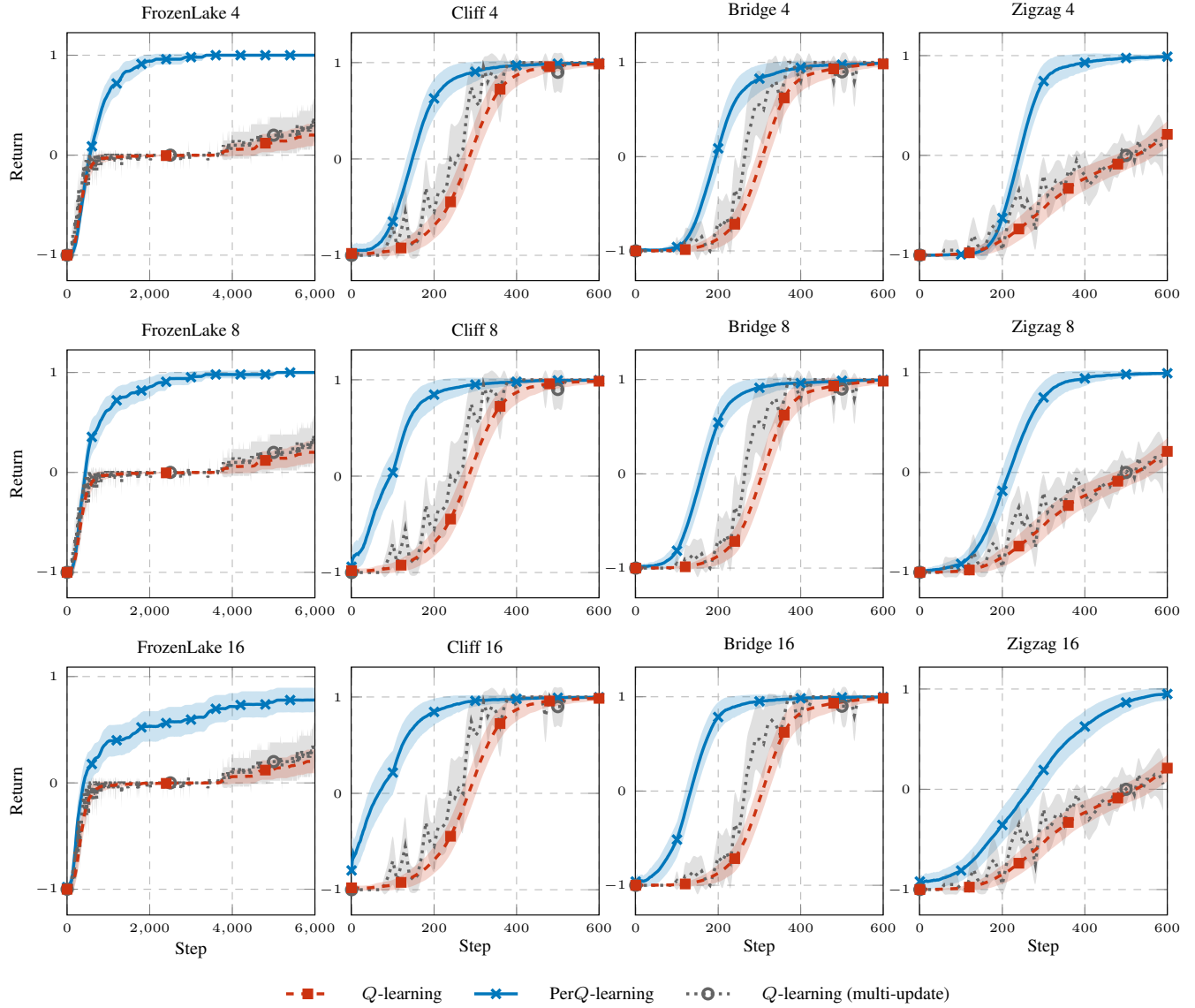


Figure 18: Results of Q -learning, TempoRL, Per Q -learning and MSA- Q -learning in different tabular environments and maximum persistences. On each row, a different maximum persistence is selected for both algorithms. 50 runs ($\text{avg} \pm 95\%$ c.i.).

In Algorithm 2, we can see that the number of total updates related is $\mathcal{O}(K_{max}^3)$. One might wonder if standard Q -learning can attain the same learning advantages with an increased number of updates: in Figure 18, we compare the results obtained for Per Q -learning with Q -learning, where the number of updates per each step has been increased for K_{max} times (the row denotes the value of K_{max}). Hence, the two algorithms have the same amount of updates. However, the increasing number of updates is not directly related to a learning improvement. If we consider Q -learning, increasing the number of updates (related to the same observed tuples) is equivalent to an increase in the learning rate, which is not necessarily related to a better learning performance. Indeed, the performances of Q -learning in its multiple-update version are not statistically better than the single-update version, only less robust.

Furthermore, the presence of multiple replay buffers allows to reduce the total number of updates linear in K_{max} in PerDQN, which is the most suited for real-world scenarios with large state-spaces. In Figure 20, we compare PerDQN with other baselines on the MountainCar environment: In the top plot, we show a comparison between our proposed approach and DQN with the same number of updates as PerDQN (denoted as DQN($\times K$)). In PerDQN, the batch size for each replay buffer is 32: in the new DQN runs, the total batch size for an update has been increased to $32 \times K_{max}$.

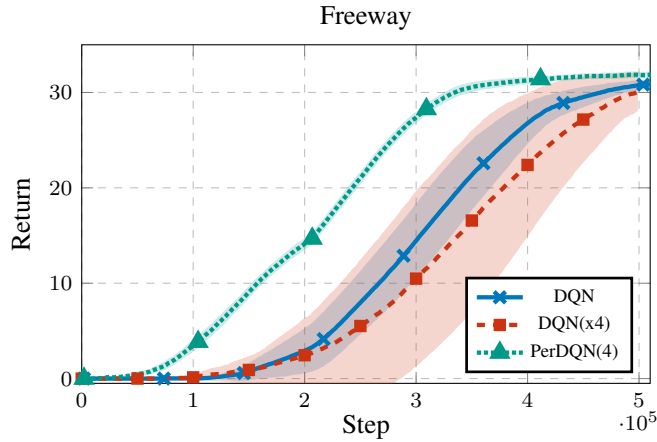


Figure 19: Freeway results: PerDQN comparison with DQN with the same global amount of tuples sampled per update as PerDQN (DQN(x4) denotes DQN where the batch size is 4 times the one adopted for classic DQN, hence with the same global batch size as PerDQN with $K_{max} = 4$).

In the middle plot, we compare PerDQN with a vanilla DQN employing ϵz -greedy exploration (Dabney, Ostrovski, and Barreto 2020). In the implementation of ϵz -greedy DQN, the exploration is performed in a similar manner as in PerDQN, as the persistence is sampled from a discrete uniform distribution in $1, \dots, K_{max}$, where K_{max} has been set to 8 and 16.

In the bottom plot, ϵz -greedy DQN is run with the same global batch size per update as in PerDQN.

In Figure 19, we compare PerDQN ($K_{max}=4$) with DQN on Freeway, with an increased batch size of a factor 4, in such a way that the total number of samples per update is the same.

In a similar fashion as with standard Q -learning, in Figure 20 the DQN curve related to $8x$ the sample size is worse (on average) than the standard version, while the $16x$ experiments see a slight improvement (with no statistical evidence). In any case, PerDQN outperforms all the compared methods. The same holds for Freeway (Figure 19), where augmenting the DQN batch size by a factor 4 does not provide improvements in the performances.

In the middle and bottom plots of Figure 20, we can see that the exploration with persistence alone (through ϵz -greedy exploration) is not enough to provide the same improvement in the learning capabilities, differently from PerDQN. Furthermore, increasing the number of updates can slightly help learning, but the resulting learning curves are still largely dominated by PerDQN.

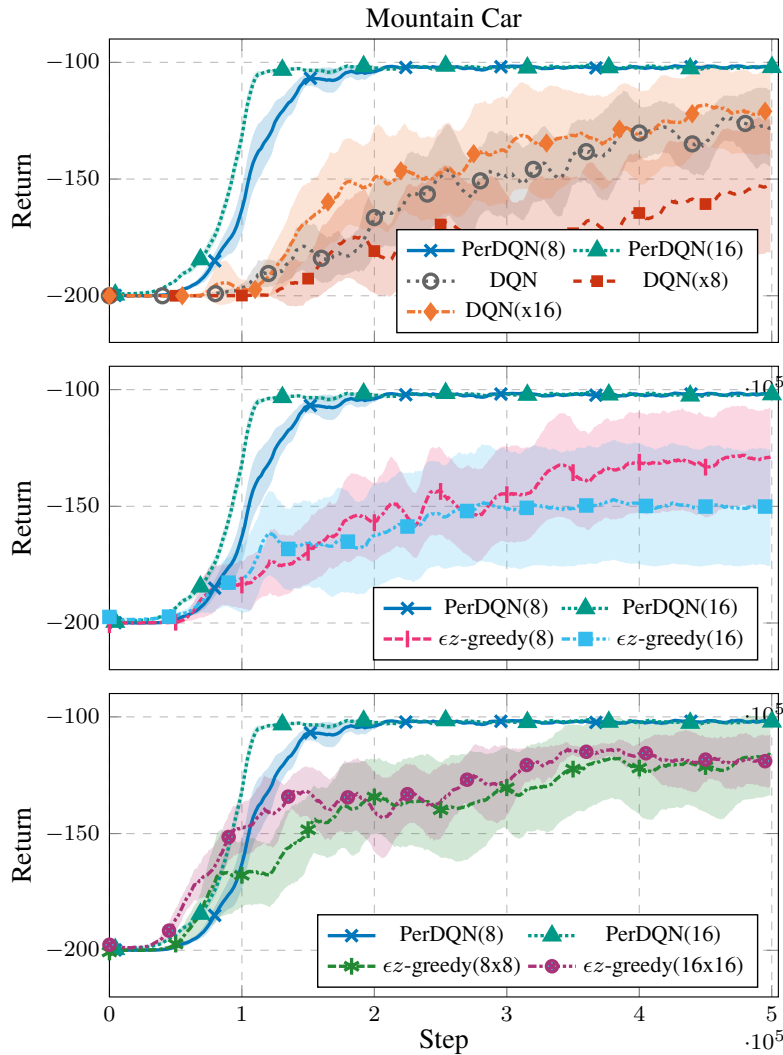


Figure 20: MountainCar results for DQN, PerDQN and ϵz -greedy DQN (10 runs, avg \pm 95% c.i.).

Top Figure: PerDQN comparison with DQN with the same global amount of tuples sampled per update as PerDQN (e.g. DQN(x8) denotes DQN where the batch size is 8 times the one adopted for classic DQN, hence with the same global batch size as PerDQN with $K_{max} = 8$).

Middle figure: PerDQN comparison with ϵz -greedy DQN, where parenthesis denote the maximum persistence in the random sampling.

Bottom figure: PerDQN comparison with ϵz -greedy DQN, with the same global amount of tuples sampled per update as PerDQN (e.g. ϵz -greedy(8x8) denotes ϵz -greedy DQN with maximum persistence for exploration equal to 8, and the batch size is 8 times the one adopted for classic DQN, hence with the same global batch size as PerDQN with $K_{max} = 8$).